Scientific Reports

https://doi.org/10.1038/s41598-026-41620-1

Article in Press

Hippopotamus optimization–tuned sigmoid PID controller for load frequency control of a two-area thermal power system with renewable energy sources

Received: 7 May 2025

Accepted: 20 February 2026

Published online: 02 March 2026

Cite this article as: Can Ö., Ayas M.Ş. & Şahin A.K. Hippopotamus optimization–tuned sigmoid PID controller for load frequency control of a two-area thermal power system with renewable energy sources. *Sci Rep* (2026). https://doi.org/10.1038/s41598-026-41620-1

Özay Can, Mustafa Şinasi Ayas & Ali Kıvanç Şahin

We are providing an unedited version of this manuscript to give early access to its findings. Before final publication, the manuscript will undergo further editing. Please note there may be errors present which affect the content, and all legal disclaimers apply.

If this paper is publishing under a Transparent Peer Review model then Peer Review reports will publish with the final article.

ARTICLE IN PRESS

© The Author(s) 2026. **Open Access** This article is licensed under a Creative Commons Attribution-NonCommercial-NoDerivatives 4.0 International License, which permits any non-commercial use, sharing, distribution and reproduction in any medium or format, as long as you give appropriate credit to the original author(s) and the source, provide a link to the Creative Commons licence, and indicate if you modified the licensed material. You do not have permission under this licence to share adapted material derived from this article or parts of it. The images or other third party material in this article are included in the article's Creative Commons licence, unless indicated otherwise in a credit line to the material. If material is not included in the article's Creative Commons licence and your intended use is not permitted by statutory regulation or exceeds the permitted use, you will need to obtain permission directly from the copyright holder. To view a copy of this licence, visit http://creativecommons.org/licenses/by-nc-nd/4.0/.

ARTICLE IN PRESS

Hippopotamus Optimization–Tuned Sigmoid PID Controller for Load Frequency Control of a Two-Area Thermal Power System with Renewable Energy Sources

1,*Özay Can, Recep Tayyip Erdogan University, Technical Sciences Vocational School, Department of Electronics and Automation, Rize, Türkiye

[2]Mustafa Şinasi Ayas, Karadeniz Technical University, Faculty of Engineering, Department of Electrical Electronics Engineering, Trabzon, Türkiye

[3]Ali Kıvanç Şahin, Erzurum Technical University, Faculty of Engineering, Department of Electrical Electronics Engineering, Erzurum, Türkiye

***Corresponding Author: **ozay.can@erdogan.edu.tr**

[1]ORCID: **https://orcid.org/0000-0003-1802-3502**
[2]ORCID: **https://orcid.org/0000-0001-8113-4817**
[3]ORCID: **https://orcid.org/0000-0003-4539-6419**

ARTICLE IN PRESS

ARTICLE IN PRESS

Hippopotamus Optimization–Tuned Sigmoid PID Controller for Load Frequency Control of a Two-Area Thermal Power System with Renewable Energy Sources

Abstract

The increasing penetration of renewable energy sources (RES) in modern interconnected power systems introduces significant challenges for load frequency control (LFC) due to increased nonlinearities, the governor dead-band (GDB) effect, parameter uncertainties, and continuous power fluctuations. These factors reduce the effectiveness of conventional fixed-gain controllers and make it difficult to maintain frequency and tie-line power deviations within acceptable limits under varying operating conditions. To address these limitations, this study proposes a sigmoid proportional-integral-derivative (SPID) controller for LFC in a two-area thermal power system integrated with RES. In the proposed approach, the controller gains are adaptively adjusted through a sigmoid-based nonlinear mapping, and the corresponding parameters are optimally tuned using the Hippopotamus Optimization (HO) algorithm by minimizing the Integral of Time-weighted Absolute Error (ITAE) performance index. The performance of the proposed HO-SPID controller is evaluated under four time-domain scenarios: a baseline case without GDB and RES, a GDB-inclusive case without RES, a case with variable RES effects, and a robustness analysis of the baseline system under simultaneous ±25% and ±50% variations in all system parameters. Additionally, to demonstrate the stability of the proposed controller, frequency-domain stability is examined using Bode analysis. Simulation results demonstrate that the proposed HO-SPID controller significantly outperforms state-of-the-art PID-based metaheuristic controllers in terms of ITAE minimization, settling time, and undershoot, while the robustness analysis under parameter uncertainties and the Bode-based frequency-domain assessment jointly confirm its stable operation.

ARTICLE IN PRESS

ARTICLE IN PRESS

Keywords: Load Frequency Control; Sigmoid Proportional-Integral-Derivative Controller; Hippopotamus Optimization; Two-Area Thermal Power System; Renewable Energy Sources; Governor Dead-Band.

1. Introduction

The fundamental objective of contemporary electrical grid systems is to ensure the provision of power to end users in a manner that is safe, dependable, and of excellent quality. In recent years, meeting this requirement has become increasingly challenging due to the rapid growth in power consumption driven by urbanization, global industrialization, and the proliferation of electronic devices. The equilibrium between energy production and consumption, which is vital for maintaining grid stability, has evolved into a complex optimization challenge that requires innovative solutions. Active power balance, a pivotal aspect of power system operation that directly influences grid frequency, represents the primary means of achieving this delicate equilibrium [1]. The grid frequency remains within permissible limits as long as the active power balance is maintained, at either 50 Hz or 60 Hz, depending on the geographical region. However, deviations from this equilibrium may lead to frequency fluctuations that, if unchecked, can harm electrical equipment and destabilize the overall power system. In other words, frequency declines when power demand exceeds generation, and frequency increases when generation exceeds demand. Such frequency-related dynamics highlight the critical need for an effective control mechanism capable of mitigating frequency deviations and preserving system stability. To address this requirement, LFC serves as a fundamental control technique that continuously monitors the system and regulates both system frequency and tie-line power exchanges within predefined limits [2].

ARTICLE IN PRESS

Despite this well-defined control objective, LFC has become significantly more challenging due to the increasing penetration of RES in modern power systems. In particular, the large-scale integration of wind turbine (WT) and photovoltaic (PV) generation into power networks traditionally dominated by thermal and hydroelectric generation introduces pronounced variability and intermittency into system dynamics. As a result, both the design of appropriate LFC control structures and the achievement of the desired regulation performance become considerably more difficult, giving rise to major challenges in LFC implementation and operation [2, 3].

To address these challenges, LFC has been extensively investigated in the literature under a wide range of operating conditions and power system configurations. Existing studies span from relatively simple single-area systems, which provide a convenient framework for controller design and fundamental performance analysis [3], to more complex multi-area interconnected power systems, including two-area [4, 5] and three-area [6] structures. Given the continuous exchange of power among interconnected regions to balance supply and demand in modern power grids, multi-area LFC studies have gained increasing importance because they more accurately capture dynamic interactions among different control areas. This shift toward interconnected multi-area operation, combined with renewable-induced variability and nonlinearities, has increased the control burden and motivated the adoption of more advanced LFC strategies.

Owing to this increased dynamic complexity, the control approaches employed in LFC have been significantly improved over time. In the early stages, traditional linear controllers such as proportional-integral (PI) [7], proportional-integral-derivative (PID) [8], and PID with filter (PID-F) [9] were widely preferred in LFC applications and played an important role for a long period. Although these controllers have demonstrated satisfactory performance in many practical scenarios, they often fall short of achieving the desired/optimal regulation performance in power systems where uncertainties and nonlinear effects become pronounced,

ARTICLE IN PRESS

particularly under high renewable penetration. Therefore, the investigation and implementation of advanced controller structures that offer greater flexibility and robustness have become increasingly important.

In this context, substantial research has focused on advanced control paradigms to mitigate the limitations of conventional linear controllers. Representative examples include fractional-order (FO) controllers (e.g., FOPI–FOPD [10]) and fuzzy logic–based schemes (e.g., FPID [11], FOFPID [12, 13], and adaptive FPID [14]). These approaches have been reported to improve LFC performance over classical PID controllers by offering enhanced flexibility and robustness. However, their effectiveness may still be constrained under nonlinear and rapidly varying operating conditions. In particular, fuzzy PID controllers often involve rule-based inference mechanisms that increase computational complexity, whereas fractional-order controllers rely on fixed fractional parameters and high-order approximations, which may introduce additional numerical burden. Consequently, there remains a clear need for alternative controller structures capable of ensuring robust and reliable LFC performance with reduced implementation complexity.

Once an appropriate controller structure is adopted to cope with the aforementioned nonlinearities and operating-condition variations, achieving the desired LFC performance becomes highly dependent on proper parameter tuning. In practical multi-area LFC applications, the tuning task typically exhibits a challenging optimization landscape due to nonlinear dynamics, coupled inter-area interactions, and RES-induced fluctuations, which often results in multimodality and limits the effectiveness of conventional gradient-based methods. For this reason, metaheuristic optimization algorithms with robust and efficient search capabilities have been widely employed for controller tuning. Representative examples include sperm swarm optimization (SSO) [15], stochastic fractal search (SFS) [16], grasshopper optimization algorithm (GOA) [17], artificial rabbits optimization (ARO) [18, 19], whale optimization algorithm (WOA) [20, 21], chaos game optimization (CGO)

ARTICLE IN PRESS

[5], dragonfly search algorithm (DSA) [22], coyote optimization algorithm (COA) [23], particle swarm optimization (PSO) [24], the RAO algorithm [25], jellyfish search optimizer (JSO) [26], fox optimizer algorithm (FOA) [27], and chaos quasi-opposition-based sea-horse optimization (CQOSHO) [28]. Although these approaches have demonstrated effectiveness in various settings, their relative performance remains problem-dependent. In line with the No-Free-Lunch theorems for optimization [29], no single method can be universally optimal across all problem classes, which motivates continued research on effective and problem-oriented optimization strategies.

Motivated by these observations, this study develops an advanced LFC framework for a two-area thermal power system integrated with WT and PV generation. By combining the sustainability of renewable energy sources with the operational reliability of conventional thermal units, the considered configuration provides a realistic representation of contemporary hybrid power systems. To cope with rapidly varying operating conditions, an SPID controller is employed. By embedding a sigmoid function within the classical PID structure, the SPID scheme enables smooth and bounded gain adaptation, allowing the controller to accommodate operating-condition variations while keeping the gains within predefined limits. This bounded adjustment mitigates excessive gain excursions and reduces the likelihood of undesirable oscillatory behavior that may arise in unbounded adaptive schemes. The parameters of the SPID controller are tuned using the HO algorithm. HO maintains a balanced exploration and exploitation mechanism in the search space, enabling reliable identification of well-tuned SPID parameters. Consequently, the proposed HO-SPID approach provides improved suppression of frequency and tie-line power deviations in the considered two-area power system. The main contributions of this study can be summarized as follows:

- An SPID controller is proposed for the first time for LFC in a two-area interconnected power system with RES integration.

ARTICLE IN PRESS

- The HO algorithm is applied for the first time to optimally tune the SPID controller parameters for two-area LFC with PV and WT generation.
- The proposed HO-tuned SPID controller is comprehensively evaluated under various operating conditions and compared with metaheuristic-based PID controllers reported in the literature. Simulation results demonstrate superior performance in terms of frequency regulation, tie-line power control, and robustness against external disturbances and system parameter variations.

The remainder of this paper is organized as follows. Section 2 describes the examined power system model, including thermal generation units, renewable energy sources, and the interconnections between the two areas. Section 3 introduces the proposed SPID controller and discusses its theoretical advantages over conventional PID controllers together with its mathematical formulation. Section 4 presents the HO algorithm by outlining its algorithmic framework and potential advantages in solving optimization problems. Section 5 presents and discusses the simulation results under various operating conditions and additionally evaluates the performance of the HO algorithm in terms of convergence behavior and solution quality. Finally, Section 6 concludes the paper by summarizing the main findings and outlining potential directions for future research.

ARTICLE IN PRESS

2. Two-Area Thermal Power System with RES

This section provides a comprehensive account of the power system model employed in the present study for the LFC process. The model reflects the intricate nature of contemporary hybrid power grids and represents a two-area non-reheat thermal power system integrated with RES [2, 16]. The system consists of two identical areas interconnected by a tie line.

The configuration of each area is as follows: Area-1 comprises a PV system, a non-reheat thermal system, and load demand. Area-2 comprises a WT system, a non-reheat thermal system, and load demand. An SPID controller, designed to regulate fluctuations in tie-line power and system frequency oscillations, is implemented in each area. To facilitate

ARTICLE IN PRESS

frequency-domain analysis, first-order transfer functions are used to represent each component within the system. The transfer functions for the components are given in Eqs. (1)-(5).

Governor:

$$G_G(s) = \frac{K_G}{\tau_G s + 1} \tag{1}$$

Turbine:

$$G_T(s) = \frac{K_T}{\tau_T s + 1} \tag{2}$$

Power System:

$$G_{PS}(s) = \frac{K_{PS}}{\tau_{PS} s + 1} \tag{3}$$

PV System:

$$G_{PV}(s) = \frac{K_{PV}}{\tau_{PV} s + 1} \tag{4}$$

Wind System:

$$G_{WT}(s) = \frac{K_{WT}}{\tau_{WT} s + 1} \tag{5}$$

ARTICLE IN PRESS

In Eqs. (1)-(5), K_G, K_T, K_{PS}, K_{PV}, and K_{WT} represent the gains of the governor, turbine, power system, PV system, and wind system, respectively. Similarly, τ_G, τ_T, τ_{PS}, τ_{PV}, and τ_{WT} represent the time constants of these components. The schematic diagram of the two-area power system under study, which displays the transfer functions of its constituent parts, is presented in Figure 1. In Figure 1, the frequency bias parameter is denoted by B, the speed control constant by R, the synchronizing coefficient of the tie-line by T_{12}, the frequency deviations for Area-1 and Area-2 by Δf_1 and Δf_2, respectively, and the tie-line power deviation between the areas by ΔP_{tie}. The parameter values for each system component corresponding to Scenario 1 (baseline system without GDB and RES) and Scenario 3 (RES-integrated system without GDB) are

ARTICLE IN PRESS

provided in Table 1. The area control error (ACE), a crucial parameter in LFC, is calculated for each area using Eqs. (6)-(7).

$$ACE_1 = B_1\Delta f_1 + \Delta P_{tie} \tag{6}$$

$$ACE_2 = B_2\Delta f_2 + \Delta P_{tie} \tag{7}$$

In order to undertake a more realistic analysis and fully examine the performance of the suggested HO-SPID controller, it is essential to take system nonlinearities such as the GDB into account. The total speed variation at which the valve position remains constant is defined as the GDB, and it is responsible for the oscillatory behavior observed in the system. The transfer function for the GDB is given in Eq. (8).

$$G_{GDB}(s) = \frac{-(0.2/\pi)s + 0.8}{\tau_G s + 1} \tag{8}$$

The incorporation of the GDB into the model improves the reliability of the control strategy evaluation by capturing real-world power-system dynamics more accurately. To reflect this modeling choice, the parameter values for each system component in Scenario 2 (including the GDB nonlinearity) are provided in Table 2.

ARTICLE IN PRESS

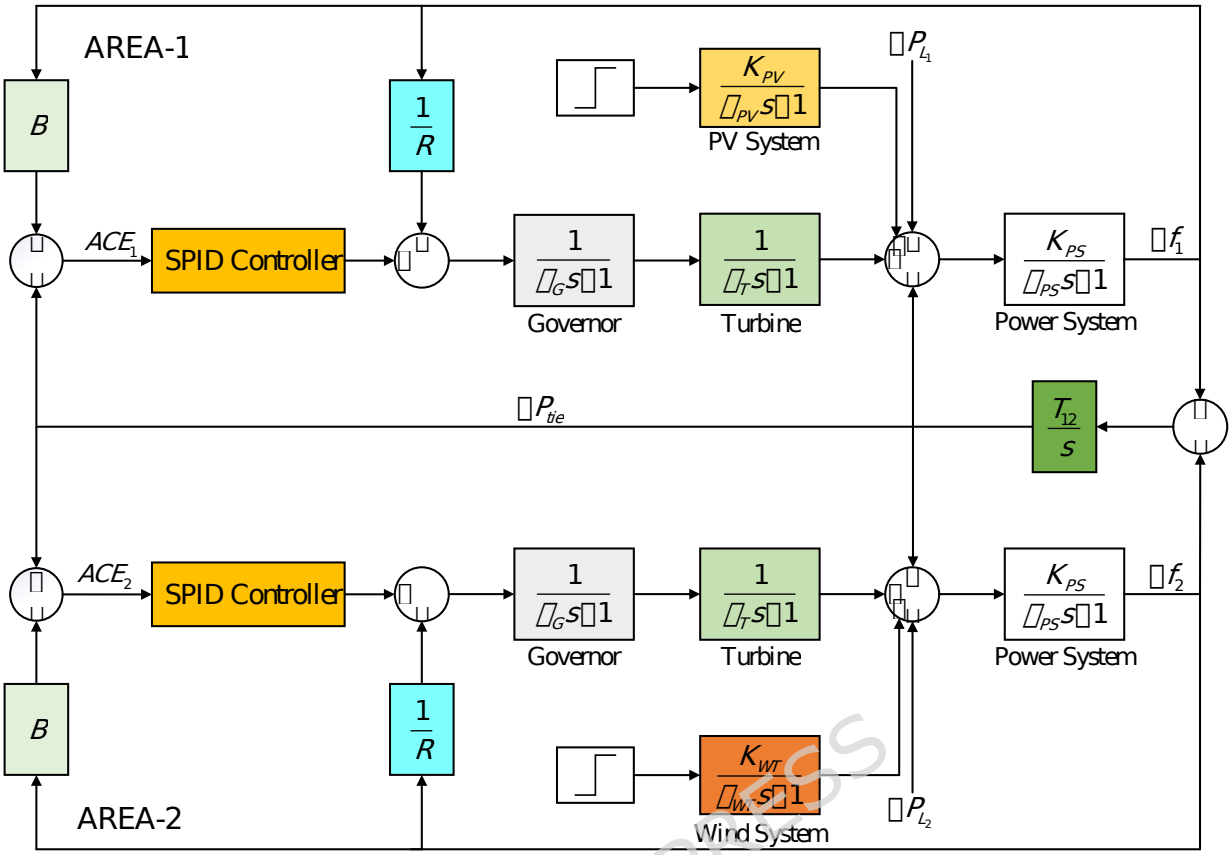

Figure 1. Two-area thermal power system with RES

Table 1. System parameter values for Scenario 1 and Scenario 3 [2]

Parameter	Value
τ_{PV}	1.3
τ_{WT}	1.5
τ_{PS}	20
τ_{G}	0.08
τ_{T}	0.3
T_{12}	0.545
K_{PS}	120
R	2.4
B	0.425
ΔP_{PV}	0.2

ARTICLE IN PRESS

ARTICLE IN PRESS

ΔP_{WT}	0.1

Table 2. System parameter values for Scenario 2 [16]

Parameter	Value
τ_G	0.2
τ_T	0.3
T_{12}	0.444
τ_{PS}	20
K_{PS}	120
R	2.4
B	0.425

ARTICLE IN PRESS

3. Controller Design

This section presents the proposed SPID controller for LFC. First, the fundamental principles of conventional PID control in the LFC framework are outlined, highlighting its main strengths and limitations. Then, the operational framework of the proposed SPID technique is described.

3.1. Conventional PID Controller

This subsection introduces the conventional PID controller used in LFC. The control input for each area is generated through proportional (K_{p_i}), integral (K_{i_i}), and derivative (K_{d_i}) actions, as given in Eq. (9). The proportional term responds to the instantaneous control error, the integral term mitigates accumulated errors to reduce steady-state deviations, and the derivative term anticipates the error trend to improve the transient response. Owing to its simple structure and ease of implementation, PID control is widely adopted in practical LFC applications in power systems. However, in interconnected multi-area power systems, frequency dynamics are strongly coupled through tie-line power exchanges, and the system exhibits pronounced variability due to nonlinearities such as the

ARTICLE IN PRESS

GDB as well as fluctuations induced by RES. Since fixed-gain PID tuning is typically performed around a nominal operating point, it cannot adequately accommodate the resulting inter-area interactions and dynamic variations as operating conditions change. Consequently, the control performance may degrade under large load disturbances and RES-induced fluctuations, which motivates the bounded adaptive SPID formulation presented in the next subsection.

$$G_{PID_l}(s) = K_{p_l} + \frac{K_{i_l}}{s} + K_{d_l}s, \quad l = 1,2 \tag{9}$$

3.2. Sigmoid PID Controller

This subsection focuses on the SPID controller, which dynamically adjusts the PID parameters based on the error dynamics and therefore differs from conventional fixed-gain PID controllers. The general structure of the SPID controller is detailed in Eq. (10), which incorporates the variables s and t, where s denotes the complex frequency variable and t denotes the physical time variable. The lower and upper bounds of the proportional, integral, and derivative gains are defined separately for the first and second SPID controllers, as specified in Eqs. (11)-(13).

For the first SPID controller, the lower bounds of the proportional, integral, and derivative parameters are K_{plb_1}, K_{ilb_1}, and K_{dlb_1}, respectively, while the corresponding upper bounds are K_{pub_1}, K_{iub_1}, and K_{dub_1}. Similarly, for the second SPID controller, the lower bounds are K_{plb_2}, K_{ilb_2}, and K_{dlb_2}, and the upper bounds are K_{pub_2}, K_{iub_2}, and K_{dub_2}. The parameters $\Delta_{p_1} = |K_{pub_1} - K_{plb_1}|$, $\Delta_{i_1} = |K_{iub_1} - K_{ilb_1}|$, $\Delta_{d_1} = |K_{dub_1} - K_{dlb_1}|$, $\Delta_{p_2} = |K_{pub_2} - K_{plb_2}|$, $\Delta_{i_2} = |K_{iub_2} - K_{ilb_2}|$, and $\Delta_{d_2} = |K_{dub_2} - K_{dlb_2}|$ represent the differences between the corresponding upper and lower gain limits and simplify the tuning of these bounds. Moreover, the parameters σ_{p_1}, σ_{i_1}, σ_{d_1}, σ_{p_2}, σ_{i_2} and σ_{d_2} determine the slope of the sigmoid function and regulate how rapidly the controller gains respond to variations in the ACE, which reflects frequency deviations and tie-line power imbalances.

Based on this sigmoid-based gain adaptation mechanism, when the ACE remains small, the controller gains vary only within a limited range,

ARTICLE IN PRESS

resulting in PID-like behavior around the nominal frequency. In contrast, when the ACE magnitude increases due to large load disturbances or the intermittent nature of renewable energy sources, the sigmoid function progressively moves toward saturation, producing a stronger gain adaptation while remaining within the predefined bounds, which enables more effective suppression of frequency deviations and tie-line power oscillations. In this way, abrupt gain variations are avoided, control effort is limited, and frequency stability in the LFC system is improved. While the sigmoid-based structure provides bounded and adaptive gain variation, its effectiveness strongly depends on the appropriate selection of the associated parameters.

Therefore, to ensure optimal performance of the LFC system, it is essential to fine-tune the 18 coefficients (K_{plb_1}, Δ_{p_1}, σ_{p_1}, K_{ilb_1}, Δ_{i_1}, σ_{i_1}, K_{dlb_1}, Δ_{d_1}, σ_{d_1}, K_{plb_2}, Δ_{p_2}, σ_{p_2}, K_{ilb_2}, Δ_{i_2}, σ_{i_2}, K_{dlb_2}, Δ_{d_2}, and σ_{d_2}) of the SPID controller. The HO algorithm is employed to determine these coefficients effectively, as described in the subsequent section.

$$G_{PID_I}(s,t) = K_{pv_I}(t) + \frac{K_{iv_I}(t)}{s} + K_{dv_I}(t)s \,, \quad I = 1,2 \tag{10}$$

$$K_{pv_I}(t) = K_{plb_I} - \left| \frac{K_{pub_I} - K_{plb_I}}{1 + e^{-\sigma_{p_I}|\Delta ACE_I(t)|}} \right| \,, \quad I = 1,2 \tag{11}$$

$$K_{iv_I}(t) = K_{ilb_I} - \left| \frac{K_{iub_I} - K_{ilb_I}}{1 + e^{-\sigma_{i_I}|\Delta ACE_I(t)|}} \right| \,, \qquad I = 1,2 \tag{12}$$

$$K_{dv_I}(t) = K_{dlb_I} - \left| \frac{K_{dub_I} - K_{dlb_I}}{1 + e^{-\sigma_{d_I}|\Delta ACE_I(t)|}} \right| \,, \quad I = 1,2 \tag{13}$$

4. HO Algorithm

ARTICLE IN PRESS

A population-based optimization technique, referred to as HO, was inspired by observations of hippopotamuses in their natural habitat [30]. In this approach, the position update of each hippopotamus is determined by the values of the decision variables, thereby offering potential solutions to the optimization problem. The HO algorithm, akin to other population-based metaheuristic algorithms, commences with randomly generated initial solutions. Subsequently, the decision-variable vector is generated using Eq. (14).

$$X_i{:}x_{ij} = lb_j + r.(ub_j - lb_j) \quad , \quad i = 1,2,...,N \quad , \quad j = 1,2,...,m \tag{14}$$

where N represents the population size, m denotes the number of decision variables, r is a random number between 0 and 1, lb and ub are the lower and upper bounds of the j-th decision variable, and X_i signifies the position of the i-th candidate solution. In this case, the population matrix is given by Eq. (15).

$$X = \begin{bmatrix} X_1 \\ \vdots \\ X_i \\ \vdots \\ X_N \end{bmatrix}_{N\times m} = \begin{bmatrix} x_{1,1} & \cdots & x_{1,j} & \cdots & x_{1,m} \\ \vdots & \ddots & \vdots & \ddots & \vdots \\ x_{i,1} & \cdots & x_{i,j} & \cdots & x_{i,m} \\ \vdots & \ddots & \vdots & \ddots & \vdots \\ x_{N,1} & \cdots & x_{N,i} & \cdots & x_{N,m} \end{bmatrix}_{N\times m} \tag{15}$$

ARTICLE IN PRESS

The algorithm consists of three main phases:

Phase 1: Hippopotamus Position Update in River or Pond (Exploration)

This phase simulates the actions of the male hippopotamuses within the herd. The location of male hippopotamuses in the river or pond is expressed in Eq. (16).

$$X_i^{Mhippo}{:}X_{ij}^{Mhippo} = x_{ij} + y_1.(Dhippo - I_1 x_{ij}) \tag{16}$$

ARTICLE IN PRESS

for $i = 1,2,\ldots, \left\lceil \frac{N}{2} \right\rceil$ and $j = 1,2,\ldots,m$

where D_{hippo} is the dominant hippopotamus with the highest fitness value. I_1 is an integer between 1 and 2, y_1 is a random number between 0 and 1, and X_i^{Mhippo} is the position of the male hippopotamus.

Phase 2: Hippopotamus Defense Against Predators (Exploration)

This phase simulates how hippopotamuses would react to predators while accounting for the vulnerability of young or sick hippopotamuses.

Phase 3: Hippopotamus Escape from Predators (Exploitation)

This phase depicts the circumstances that hippopotamuses encounter when they are unable to repel predators and attempt to flee to the nearest body of water. The referenced study [30] presents a flowchart, a comprehensive mathematical model, and supplementary information regarding the HO method.

ARTICLE IN PRESS

4.1. Tuning of the SPID Controller Using the HO Algorithm in a Two-Area Thermal Power System with RES Integration

In the optimization framework, the population size, the maximum number of fitness function evaluations, and the number of decision variables for the SPID controller are set to 50, 10,000, and 18, respectively. The algorithm incorporates lower and upper bounds for each parameter of the SPID controller within the range [0.2, 5], ensuring that the parameters remain within these limits throughout the optimization process. The parameter values have been incorporated into the HO algorithm implemented in the MATLAB environment. Figure 2 illustrates the implementation procedure of the HO algorithm for tuning the SPID controller in a two-area thermal power system with RES integration. The optimization process is based on the objective function given in Eq. (17),

ARTICLE IN PRESS

namely, the ITAE, which evaluates and guides parameter tuning to achieve optimal system performance.

$$OF = \int_0^t (|\Delta f_1 + \Delta f_2 + \Delta P_{tie}|)\, tdt \quad (17)$$

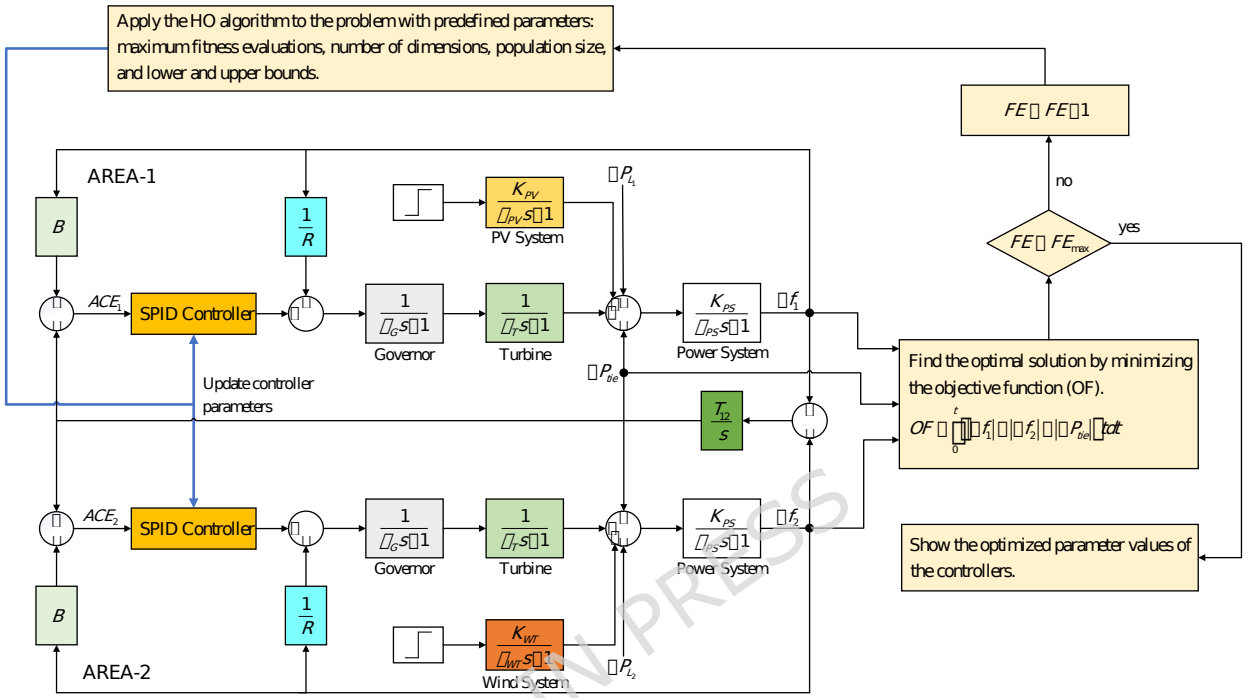

Figure 2. HO-based tuning of the SPID controller in a two-area thermal power system with RES integration.

ARTICLE IN PRESS

5. Simulation Studies and Numerical Results

To evaluate the effectiveness of the HO algorithm used in this study, its performance is compared with that of various metaheuristic algorithms reported in the LFC literature [31, 32]. As a preliminary validation step, the algorithm is tested on nine different benchmark functions, after which a comprehensive time-domain analysis of the proposed controller and optimization method is presented in the context of LFC. The time-domain simulation studies focus on four different scenarios, each specifically designed to evaluate different aspects of system functionality and controller performance. The four scenarios are defined as follows:

ARTICLE IN PRESS

- Scenario 1 (Baseline): Evaluates the fundamental behavior of the system in the absence of GDB effects and RES integration.
- Scenario 2 (GDB-Inclusive): Investigates the system response by introducing GDB nonlinearities while excluding RES impacts.
- Scenario 3 (RES-Integrated): Incorporates realistic RES dynamic models to reflect contemporary power-system characteristics while neglecting the GDB effect.
- Scenario 4 (Robustness Analysis): Assesses the robustness of the proposed approach under parametric uncertainties by simultaneously varying key system parameters and time constants by ±25% and ±50%.

For each scenario, the optimal controller gains are obtained and given in Table 3. Finally, to complement the time-domain assessment, Bode analysis is employed to examine the frequency-domain stability of the LFC system with the proposed controller.

Table 3. The optimal controller parameters for each scenario

Scenario No	Area-1									Area-2								
	K_{plb_1}	Δ_{p_1}	σ_{p_1}	K_{ilb_1}	Δ_{i_1}	σ_{i_1}	K_{dlb_1}	Δ_{d_1}	σ_{d_1}	K_{plb_2}	Δ_{p_2}	σ_{p_2}	K_{ilb_2}	Δ_{i_2}	σ_{i_2}	K_{dlb_2}	Δ_{d_2}	σ_{d_2}
I	4.9359	0.6649	3.9151	5	0.2	4.5736	1.2241	0.2056	2.0307	1.5876	0.2044	2.0949	4.2314	1.6242	4.9991	0.6286	0.2036	4.3050
II	3.6560	4.6130	3.3844	4.9740	3.4727	4.9860	2.4075	3.0650	4.6150	3.2760	4.4695	4.5686	2.2593	3.1387	3.6581	3.2568	3.1610	1.5381
III	Same controller parameters with Scenario I.																	
IV	Same controller parameters with Scenario I.																	

ARTICLE IN PRESS

5.1. Performance Comparison of Metaheuristic Algorithms

In this subsection, the performance of the HO algorithm used to tune the SPID controller [33] is compared against several metaheuristic algorithms previously reported for PID tuning in the same LFC system. These algorithms include the Fire Hawk Optimizer [34], Brown Bear Optimization (BOA) [35], Grey Wolf Optimizer (GWO) [36], Particle Swarm Optimization (PSO) [37], and Differential Evolution (DE) [38].

To ensure a rigorous and unbiased comparison, the maximum number of fitness evaluations is set to 100,000 for each algorithm. A total of nine benchmark functions is used to comprehensively evaluate algorithm performance. The mathematical formulations of these benchmark functions, along with details of their problem dimensions, search-space

bounds (Range), and global optimum (f_{min}), are presented in Table 4. Performance metrics, including means, standard deviations, and best values, are computed over 20 independent runs for each benchmark function to ensure statistical reliability.

Table 4. Benchmark functions used to compare algorithm performances

Functions	m	Range	Mathematical Description	f_{min}
Sphere	50	[-100, 100]	$f_1(x) = \sum_{i=1}^{m} x_i^2$	0
Schwefel 2.22.	50	[-100, 100]	$f_2(x) = \sum_{i=1}^{m} \lvert x_i \rvert + \prod_{i=1}^{m} \lvert x_i \rvert$	0
Schwefel 1.2.	50	[-100, 100]	$f_3(x) = \sum_{i=1}^{m} \left(\sum_{j=1}^{i} x_j \right)^2$	0
Schwefel 2.21.	50	[-100,100]	$f_4(x) = \max(\lvert x_i \rvert, 1 \le i \le m)$	0
Step	50	[-100,100]	$f_5(x) = \sum_{i=1}^{m} (\lfloor x_i + 0.5 \rfloor)^2$	0
Quartic with noise	50	[-1.28,1.28]	$f_6(x) = \sum_{i=1}^{m} i x_i^4 + \text{random}[0,1)$	0
Rastrigin	50	[-5.12, 5.12]	$f_7(x) = \sum_{i=1}^{m} \left[x_i^2 - 10\cos(2\pi x_i) + 10 \right]$	0
Ackley	50	[-32, 32]	$f_8(x) = -20\exp\left(-0.2\sqrt{\frac{1}{m}\sum_{i=1}^{m} x_i^2} \right) - \exp\left(\frac{1}{m}\sum_{i=1}^{m} \cos(2\pi x_i) \right) + 20 + e$	0
Griewank	50	[-600, 600]	$f_9(x) = \frac{1}{4000}\sum_{i=1}^{m} x_i^2 - \prod_{i=1}^{m} \cos\left(\frac{x_i}{\sqrt{i}} \right) + 1$	0

ARTICLE IN PRESS

Table 5 presents the best, mean, and standard deviation values of each algorithm for the nine benchmark functions. The results indicate that:

- Best value: The HO algorithm consistently achieved lower best objective values than the other algorithms, except for the f_5 benchmark function.

ARTICLE IN PRESS

- Lower mean value: Except for the f_5 function, the HO algorithm achieved lower average objective values, indicating improved convergence behavior across fitness evaluations.
- Smaller standard deviation value: Except for the f_5 function, the HO algorithm exhibited lower variability across independent runs, indicating more consistent performance.

In addition to the numerical results reported in Table 5, Figure 3 presents the best convergence profiles obtained for each benchmark function, with subfigures (a)-(i) corresponding to benchmark functions f_1-f_9, respectively. These comparative results provide a basis for assessing the suitability of candidate optimization algorithms, as they reveal the extent to which the algorithms can maintain an appropriate exploration–exploitation balance and achieve consistent convergence in high-dimensional problems. In this context, tuning an SPID controller, which involves a large number of adjustable parameters, requires a reliable and stable optimization approach. Based on the comparative evaluations conducted on benchmark functions f_1-f_9, HO is observed to exhibit more consistent and competitive performance than FHO, GWO, BOA, PSO, and DE. Therefore, it is selected for the SPID-controlled LFC system.

ARTICLE IN PRESS

ARTICLE IN PRESS

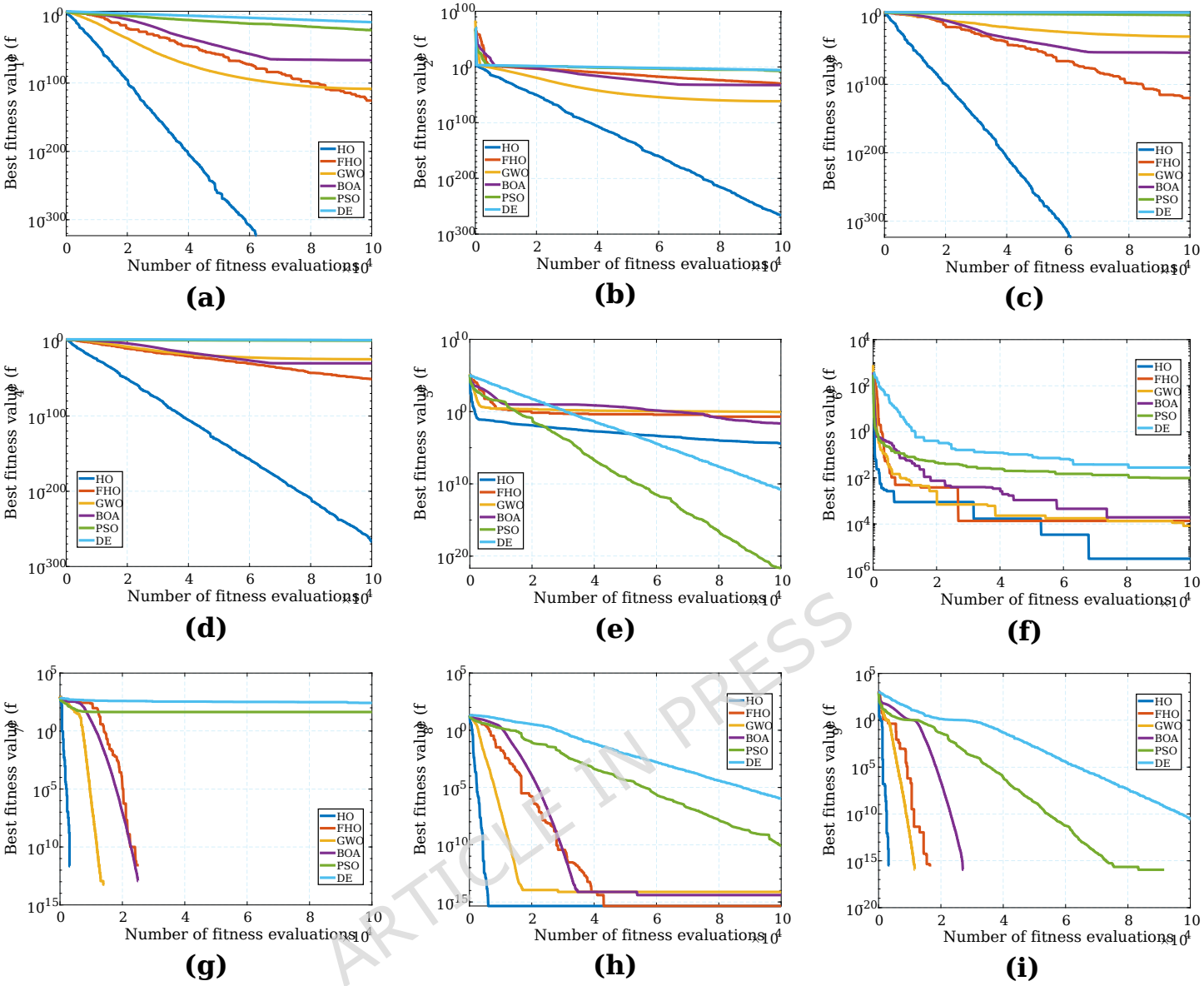

Figure 3. Best convergence profiles of the HO, FHO, GWO, BOA, PSO, and DE algorithms, where subfigures (a)–(i) correspond to benchmark functions f_1-f_9

Table 5. Comparative statistical analysis of HO, FHO, GWO, BOA, PSO, and DE metaheuristics on classical benchmark functions, evaluated over

ARTICLE IN PRESS

20 independent runs with a maximum of 100,000 function evaluations per run

Benchmark Functions	Performance Measures	HO	FHO [34]	GWO [36]	BOA [35]	PSO [37]	DE [38]
f_1	Mean	0	1.6367e-112	1.5671e-107	4.0327e-65	6.6139e-20	4.9592e-11
	Standard deviation	0	6.9090e-112	2.0401e-107	8.3615e-65	1.9045e-19	1.9742e-11
	Best	0	2.8659e-126	4.1167e-109	3.6907e-67	2.754e-23	1.5039e-11
f_2	Mean	8.9098e-257	2.3629e-27	2.1218e-61	7.2154e-33	7.4980e-03	9.183e-05
	Standard deviation	0	8.3027e-27	2.2285e-61	4.6585e-33	2.9987e-02	1.1783e-04
	Best	3.2855e-267	1.2939e-30	2.5067e-62	2.7143e-33	6.4301e-08	2.7148e-06
f_3	Mean	0	1.7160e-110	4.8795e-23	6.8117e-53	6.3006e+01	9.6768e+04
	Standard deviation	0	5.0388e-110	4.8795e-23	8.2892e-53	2.7563e+01	8.7314e+03
	Best	0	3.0572e-121	5.2286e-31	1.7384e-54	1.8775e+01	7.2691e+04
f_4	Mean	2.1246e-257	5.5237e-45	1.2404e-23	7.6439e-30	2.7703	1.0604e+01
	Standard deviation	0	1.7966e-44	2.084e-23	3.7701e-30	9.1667e-01	1.988
	Best	9.4131e-269	9.8825e-52	3.0963e-25	1.3685e-30	1.4419	7.4047
f_5	Mean	1.1984e-04	7.395e-01	1.6176	2.063e-01	2.049e-19	3.7039e-11
	Standard deviation	8.9081e-05	1.306	3.8952e-01	1.528e-01	8.5994e-19	1.6570e-11
	Best	4.0049e-05	1.9840e-01	8.8481e-01	2.3e-02	2.2040e-22	1.7042e-11
f_6	Mean	6.8985e-05	1.1e-03	4.3334e-04	4.2311e-04	1.6918e-02	4.1581e-02
	Standard deviation	6.0929e-05	6.0467e-04	2.8776e-04	1.4686e-04	4.4326e-03	7.9913e-03
	Best	3.0871e-06	1.3513e-04	8.2386e-05	1.9322e-04	9.7816e-03	2.7992e-02
f_7	Mean	0	0	0	2.5245e+01	7.3726e+01	2.9593e+02
	Standard deviation	0	0	0	1.7821e+01	2.4522e+01	1.1959e+01
	Best	0	0	0	0	4.3778e+01	2.6697e+02
f_8	Mean	4.4409e-16	4.4409e-16	1.3589e-14	4.7073e-15	1.541	1.7797e-06
	Standard deviation	0	0	2.6031e-15	1.4580e-15	5.7667e-01	4.3557e-07
	Best	4.4409e-16	4.4409e-16	7.5495e-15	3.9968e-15	8.3237e-11	1.1059e-06
f_9	Mean	0	0	4.0625e-04	1.7e-03	1.1673e-02	1.0234e-10
	Standard deviation	0	0	1.8168e-03	3.6e-03	1.3753e-02	1.7356e-10
	Best	0	0	0	0	0	2.8241e-11

5.2. Scenario I: ±10% pu Load Change without RES and GDB

ARTICLE IN PRESS

In this scenario, the system response to a 0.1 pu load change applied at t = 10 s in Area-1 is examined without considering RES integration and GDB nonlinearity. This baseline configuration provides a reference condition for consistently evaluating the effects of subsequent scenarios. Within this reference setting, the dynamic responses of Area-1, Area-2, and tie-line power are illustrated in Fig. 4. Table 6 provides the key performance metrics obtained from these responses, namely the settling time (t_s), maximum undershoot (MU), and the ITAE. The proposed HO-SPID controller achieves settling times of 11.312 s, 12.693 s, and 11.998 s for Δf_1, Δf_2, and ΔP_{tie}, respectively. These values are substantially lower than those obtained using other metaheuristic-based PID methods. For example, the closest competitor (BOA-PID [2]) yields corresponding values of 14.351 s, 15.593 s, and 14.839 s, indicating improvements of approximately 21.15%, 18.61%, and 19.15%, respectively. These results demonstrate the enhanced capability of the HO-SPID controller to accelerate system stabilization following the load disturbance. In addition to the settling-time improvement, the HO-SPID controller exhibits favorable damping characteristics. It achieves MU $\times 10^{-2}$ values of 6.504 Hz for Δf_1, 2.529 Hz for Δf_2, and 0.870 pu.MW for ΔP_{tie}. These values are consistently smaller than those obtained with BOA-PID [2], PSO-PID [2], and GWO-PID [2], indicating more effective suppression of oscillatory components in both frequency and tie-line power deviations. Complementing the MU assessment, the ITAE metric provides a broader measure of dynamic performance. The HO-SPID controller achieves an ITAE value of 0.6330, confirming its superior transient behavior and improved disturbance-rejection capability under the baseline load-change scenario compared with other metaheuristic-based PID approaches.

ARTICLE IN PRESS

ARTICLE IN PRESS

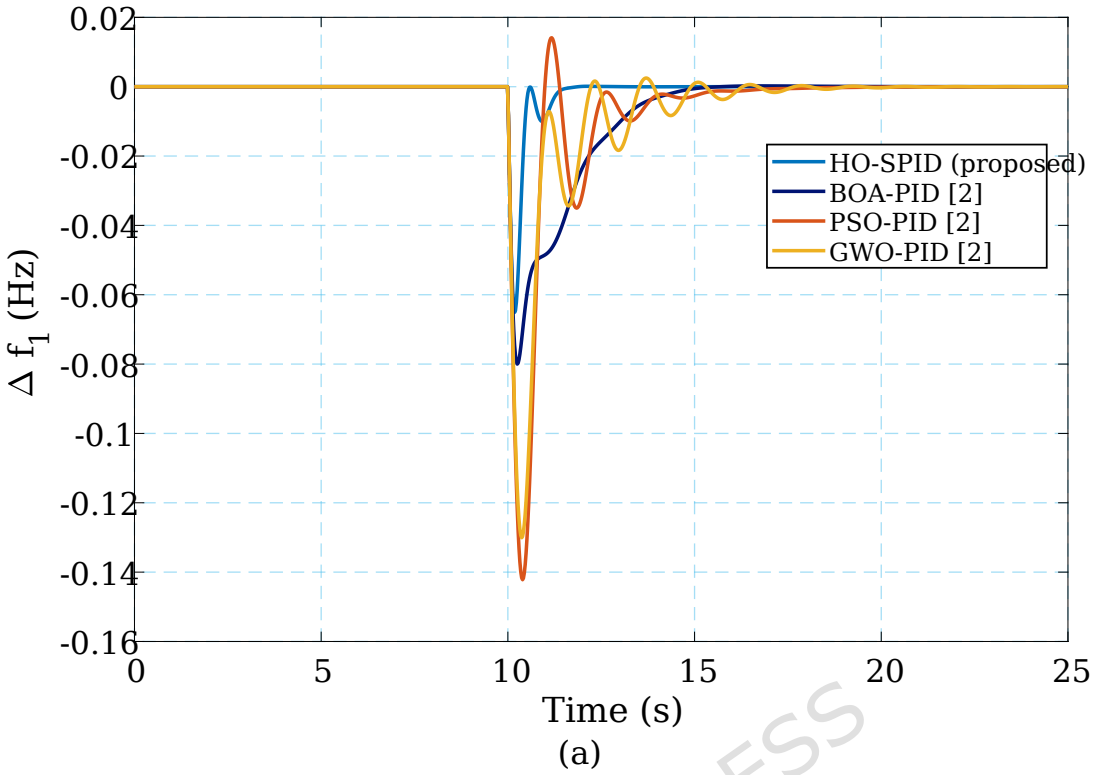

(a)

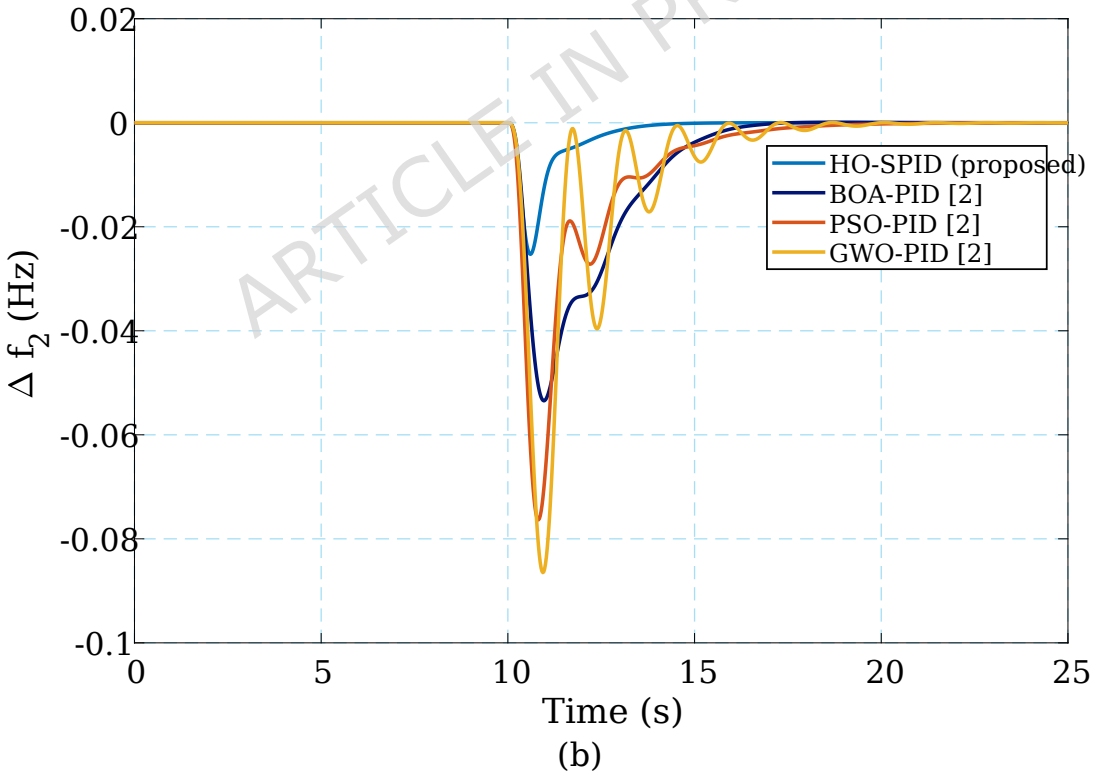

(b)

ARTICLE IN PRESS

ARTICLE IN PRESS

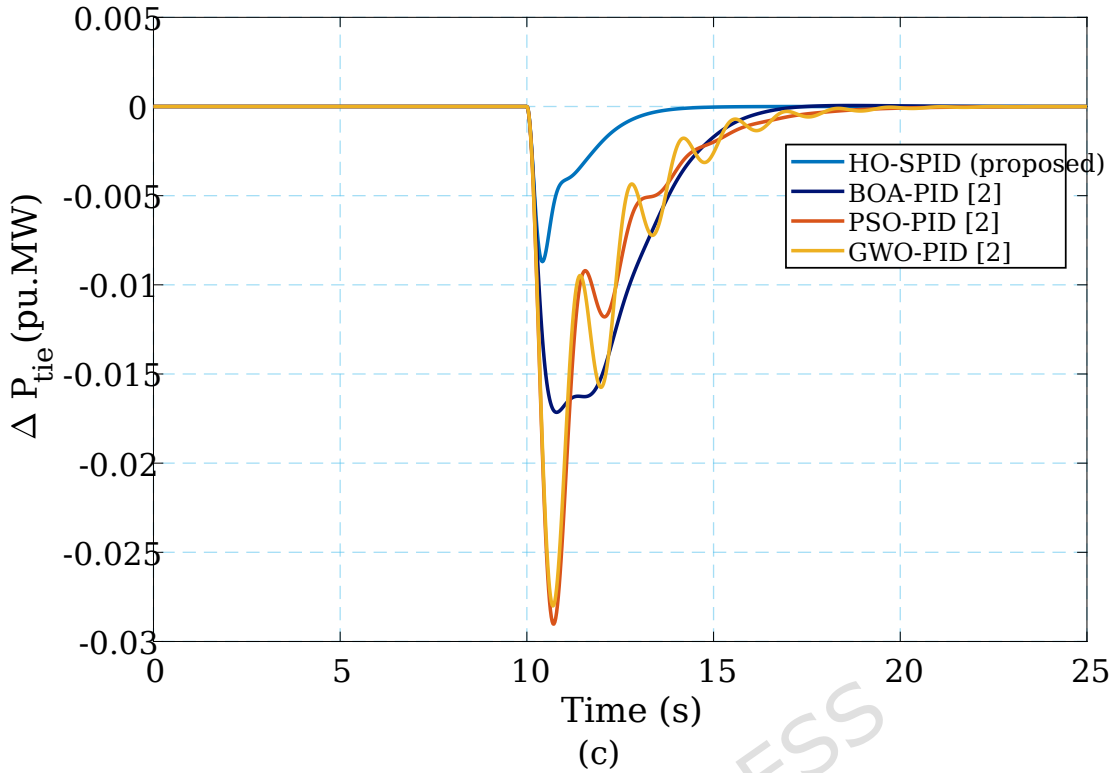

(c)

Figure 4. System responses for Scenario I, a) area-1, b) area-2, c) tie-line

Table 6. Comparison of system performance metrics for different controllers under Scenario I (10% pu load change without GDB and RES effects)

Controller	t_s (s)			MU × 10^{-2} (Hz)		MU (pu.MW)	ITAE
	Δf_1	Δf_2	ΔP_{tie}	Δf_1	Δf_2	ΔP_{tie}	
HO-SPID (proposed)	11.312	12.693	11.998	6.504	2.529	0.870	0.6330
BOA-PID [2]	14.351	15.593	14.839	7.999	5.345	1.715	3.3790
PSO-PID [2]	15.187	16.291	14.993	14.218	7.635	2.903	3.4109
GWO-PID [2]	16.050	16.866	16.866	13.006	8.649	2.801	3.4159

In addition to the load-increase scenario analyzed above, it is also essential to evaluate the controller performance under load-decrease conditions, since practical power systems experience demand variations in both directions and thus require effective regulation. Figure 5 depicts the dynamic responses of the system to a -0.01 pu load change applied in Area-

ARTICLE IN PRESS

1 at $t = 10$ s. The results indicate that the proposed HO-SPID controller keeps the frequency and tie-line power deviations within acceptable limits and provides fast damping behavior, consistent with the performance observed under load-increase conditions. Overall, this bidirectional evaluation further supports the robustness of the controller in coping with both positive and negative load disturbances. To further examine this robustness, simultaneous multi-area disturbances are considered.

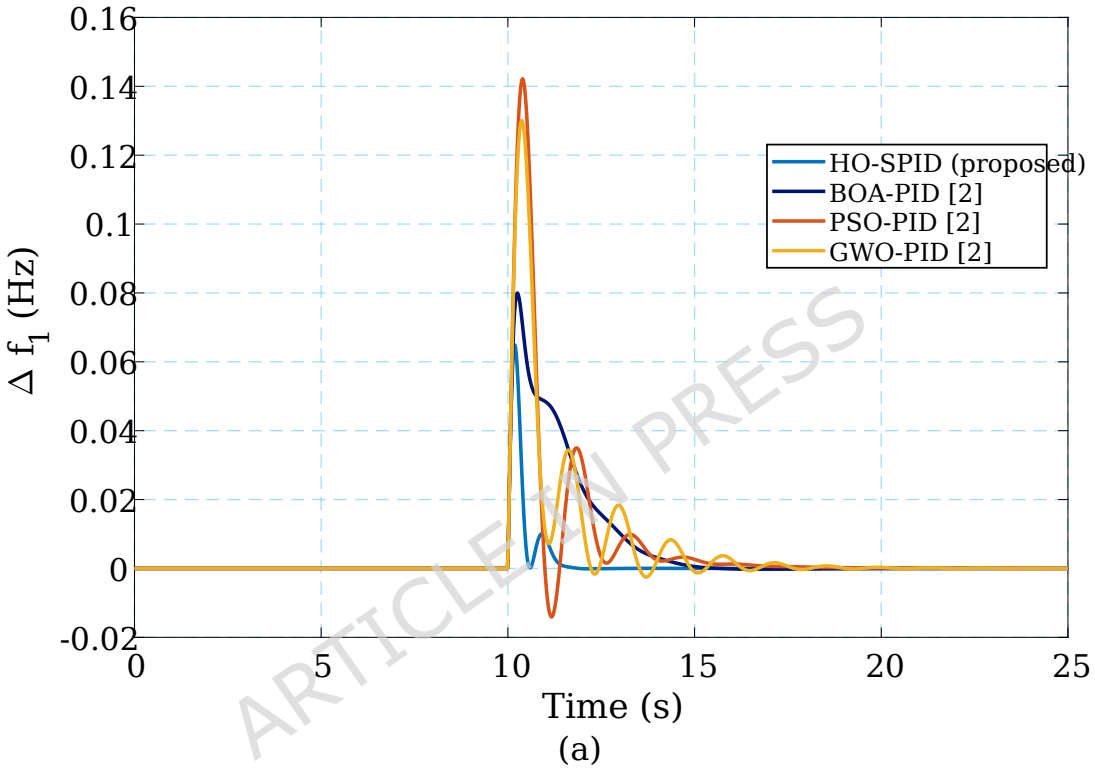

(a)

ARTICLE IN PRESS

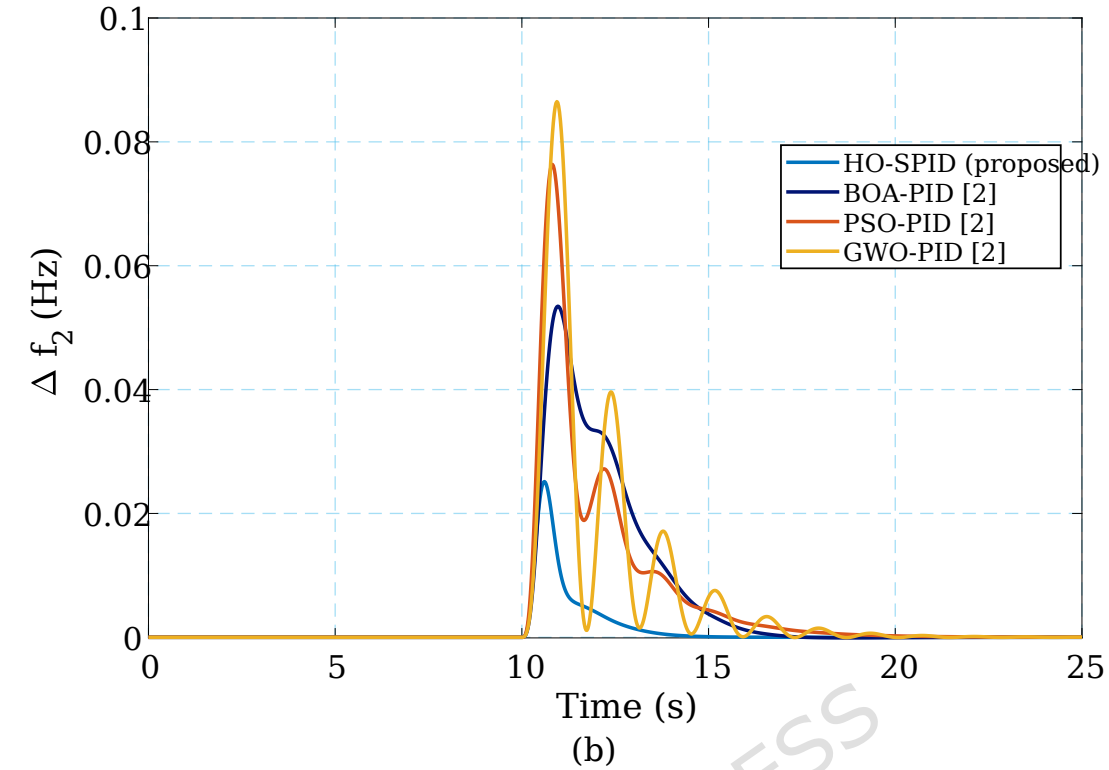

(b)

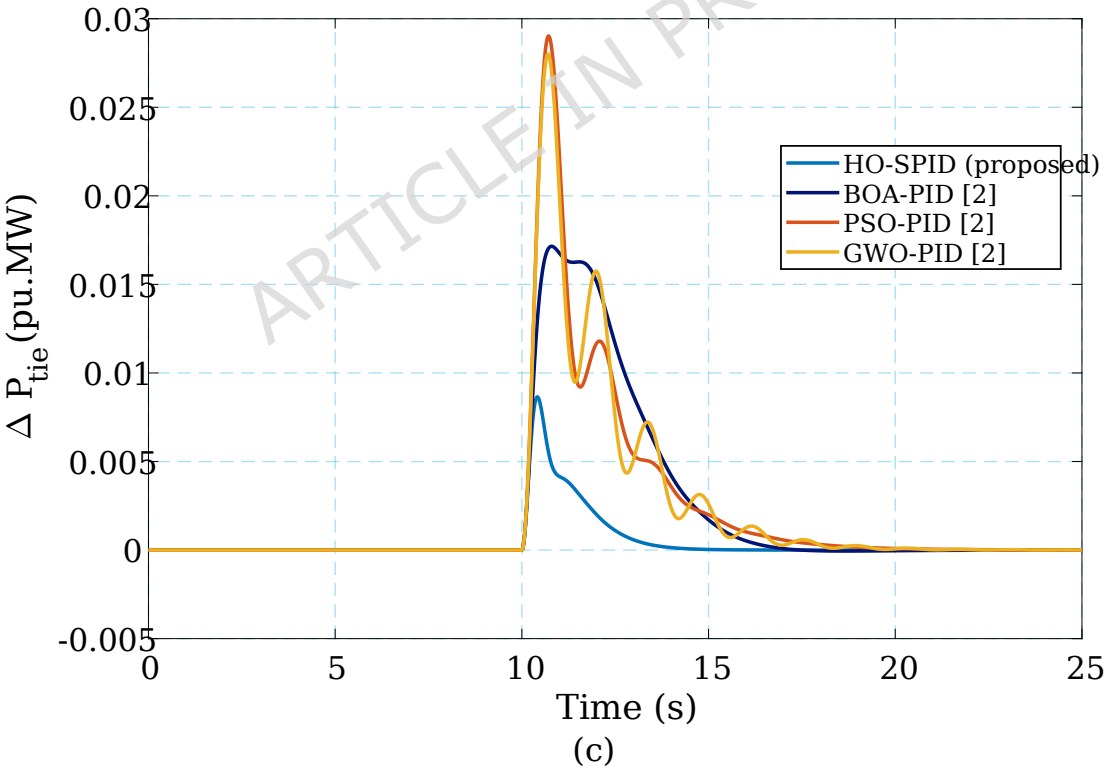

(c)

Figure 5. System responses for -10% pu load change, a) area-1, b) area-2, c) tie-line

As shown in Fig. 6, simultaneous load increases of 0.1 pu in Area-1 and 0.2 pu in Area-2 are applied at t = 10 s, and the corresponding dynamic

ARTICLE IN PRESS

responses are recorded. The results indicate that the proposed HO-SPID controller effectively attenuates frequency deviations and keeps tie-line power oscillations within acceptable limits. Notably, the controller preserves fast damping and short settling times despite concurrent disturbances of different magnitudes in both areas, which further substantiates its robustness in maintaining overall system stability. This capability is particularly relevant to practical power-system operation, where simultaneous load variations across interconnected areas can frequently occur.

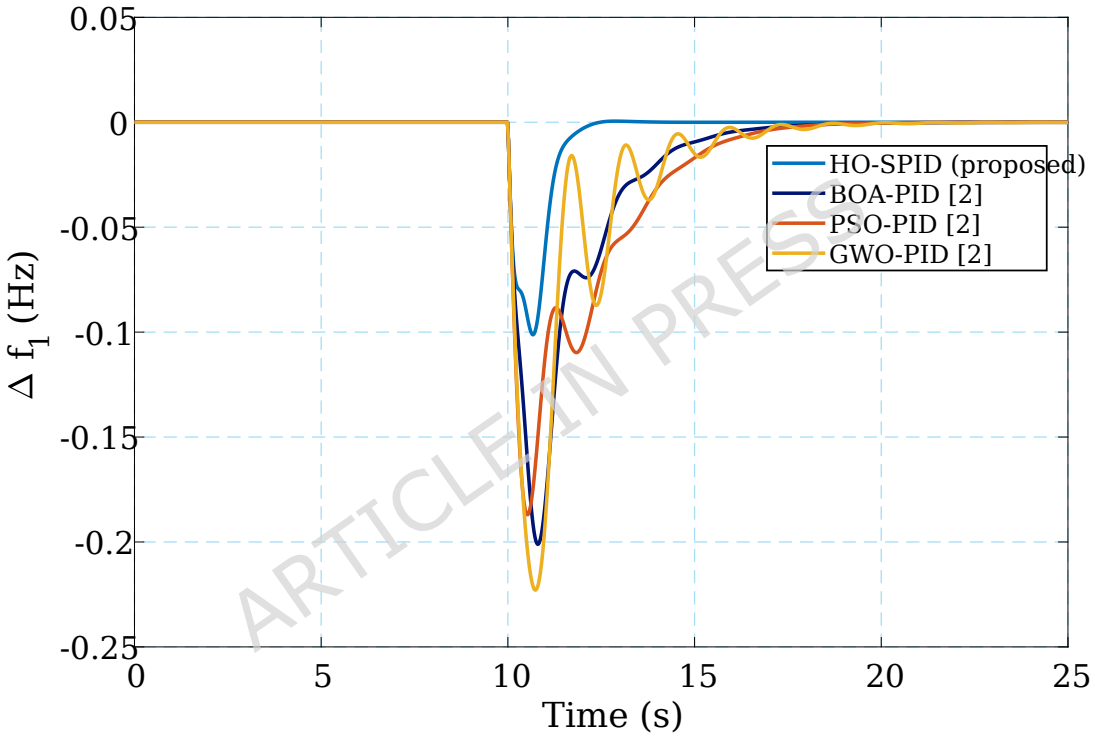

(a)

ARTICLE IN PRESS

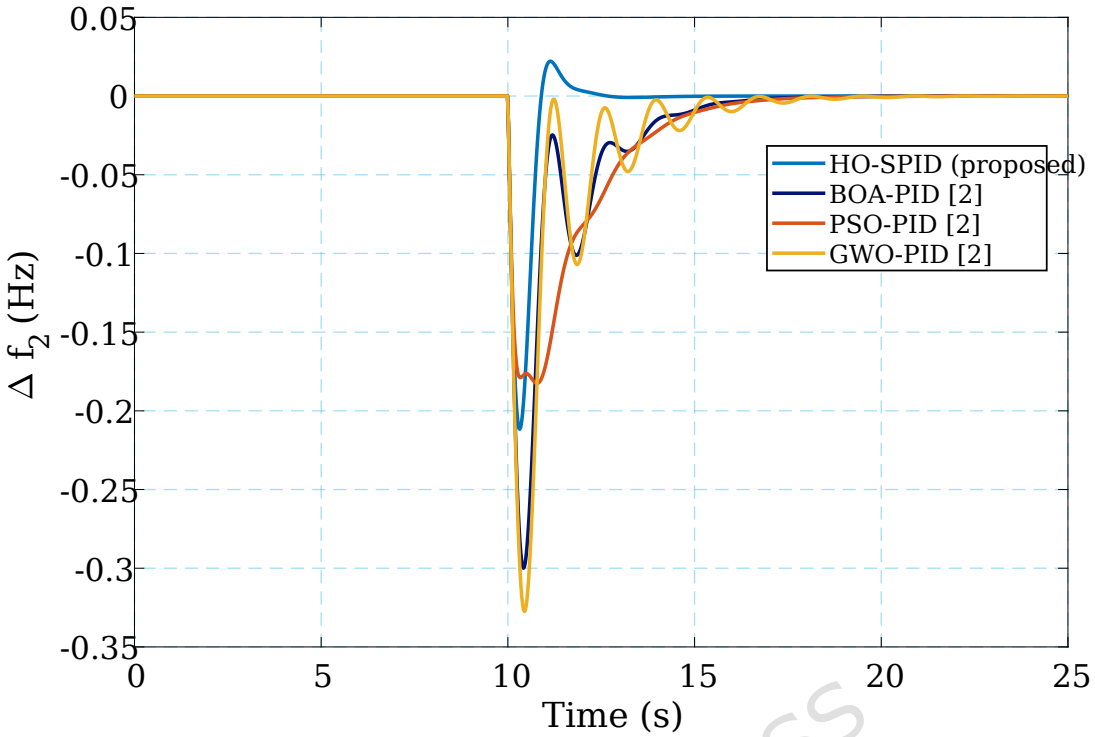

(b)

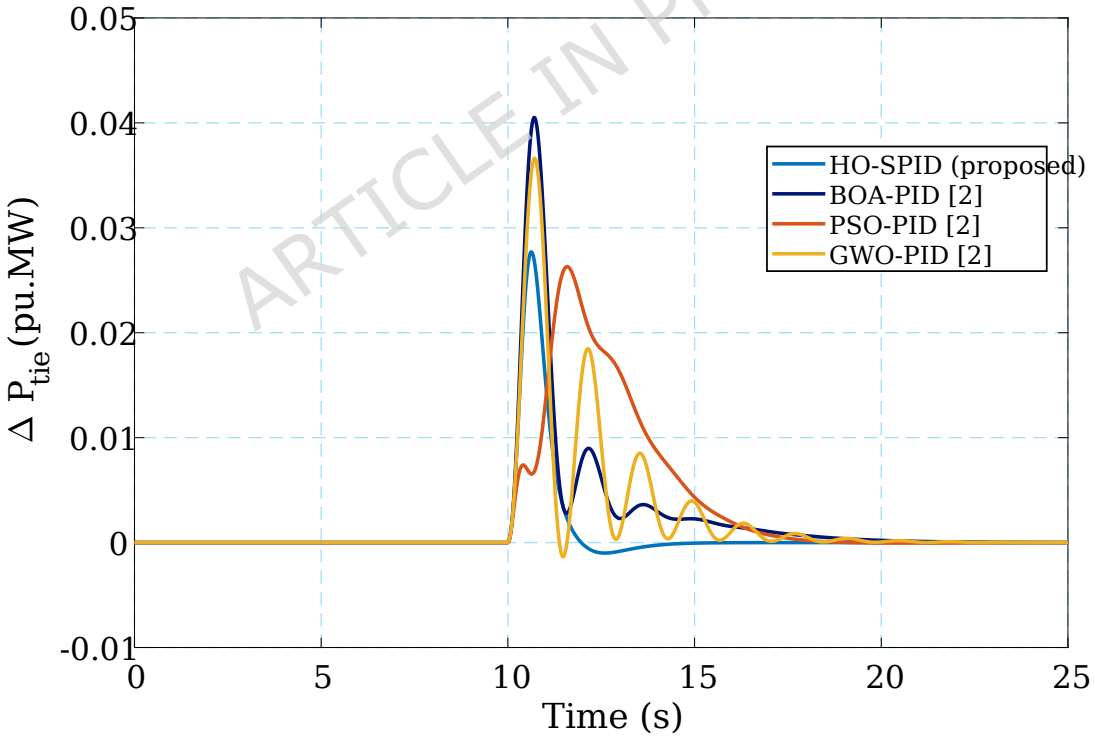

(c)

Figure 6. System responses for load change in both areas, a) area-1, b) area-2, c) tie-line

ARTICLE IN PRESS

5.3. Scenario II: 1% pu Load Change with GDB

To obtain a more accurate understanding of system behavior, it is necessary to consider the influence of the GDB in power system analysis. In this scenario, simulations incorporating the effect of the GDB are carried out in order to evaluate system performance under more realistic operating conditions. The system responses obtained from these simulations are presented in Figure 7, and the numerical data extracted from these responses are provided in Table 7. A comprehensive examination of Table 7 offers valuable insights into the effectiveness of the HO-SPID controller when compared with alternative approaches. Accordingly, in terms of settling time, the HO-SPID controller exhibits superior performance across all parameters (Δf_1, Δf_2, and ΔP_{tie}). When compared with the next-best method, the HO-SPID controller provides improvements of 34.59% for Δf_1 relative to ISFS-PID [16], 25.41% for Δf_2 relative to DE-PID [31], and 51.10% for ΔP_{tie} relative to FHO-PID [32]. With respect to maximum undershoot, the HO-SPID controller also demonstrates competitive behavior by achieving the lowest MU values among all compared methods. For Δf_1, it provides a 4.76% reduction relative to ISFS-PID [16]. For Δf_2, it achieves a 16.36% reduction relative to ISFS-PID [16]. For ΔP_{tie}, the HO-SPID controller yields a 14.96% reduction compared with FHO-PID [32]. Furthermore, the HO-SPID controller attains the lowest ITAE value of 0.0215, offering a 60.26% improvement relative to the next-best method, FHO-PID [32].

Overall, the results in Table 7 indicate that the HO-SPID controller delivers strong performance across multiple dynamic metrics under the influence of the GDB, particularly in terms of settling time, maximum undershoot, and ITAE, while maintaining a competitive dynamic response.

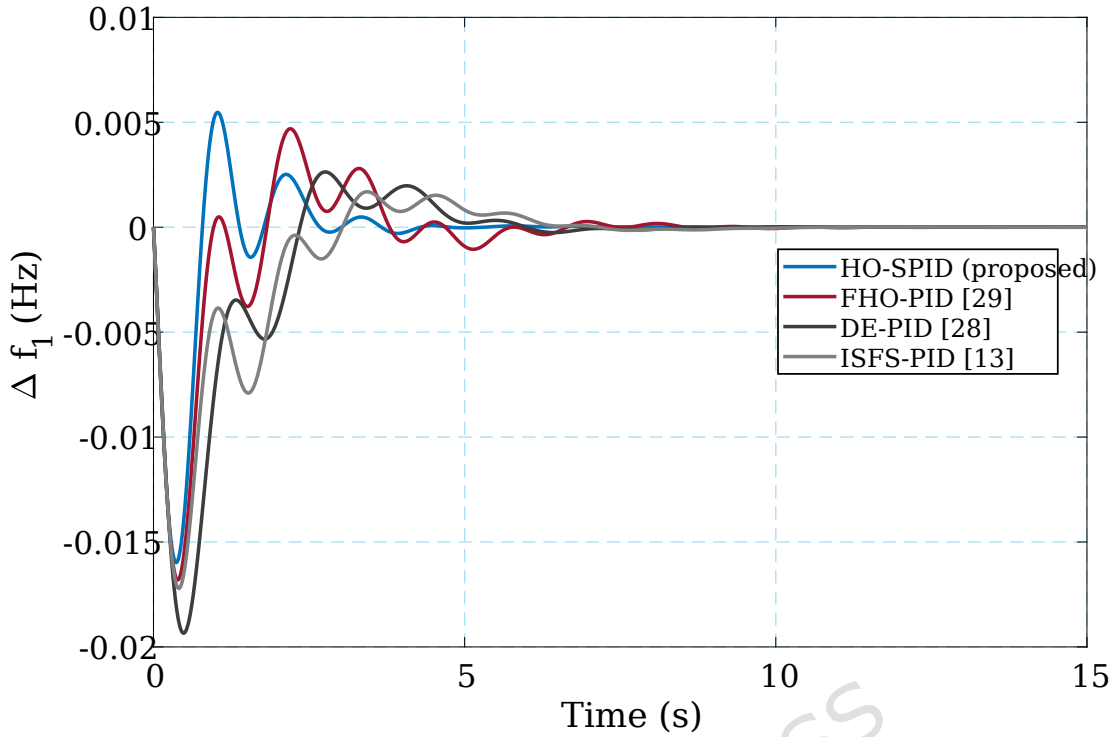

(a)

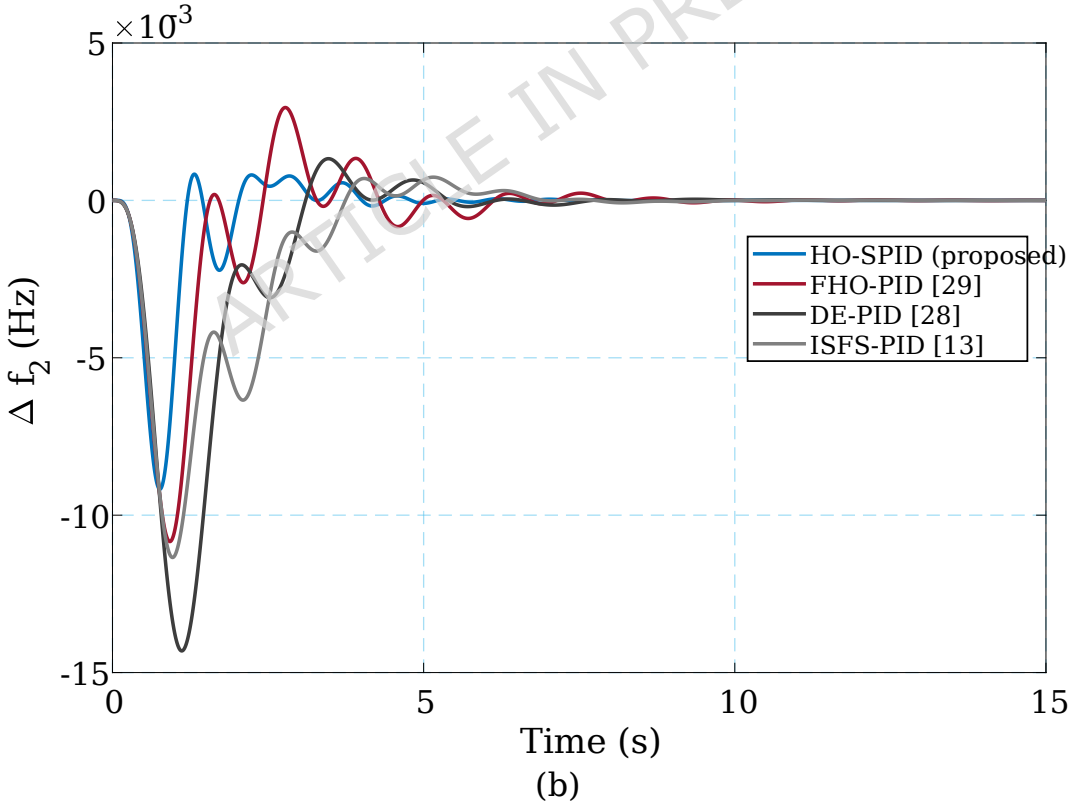

(b)

ARTICLE IN PRESS

ARTICLE IN PRESS

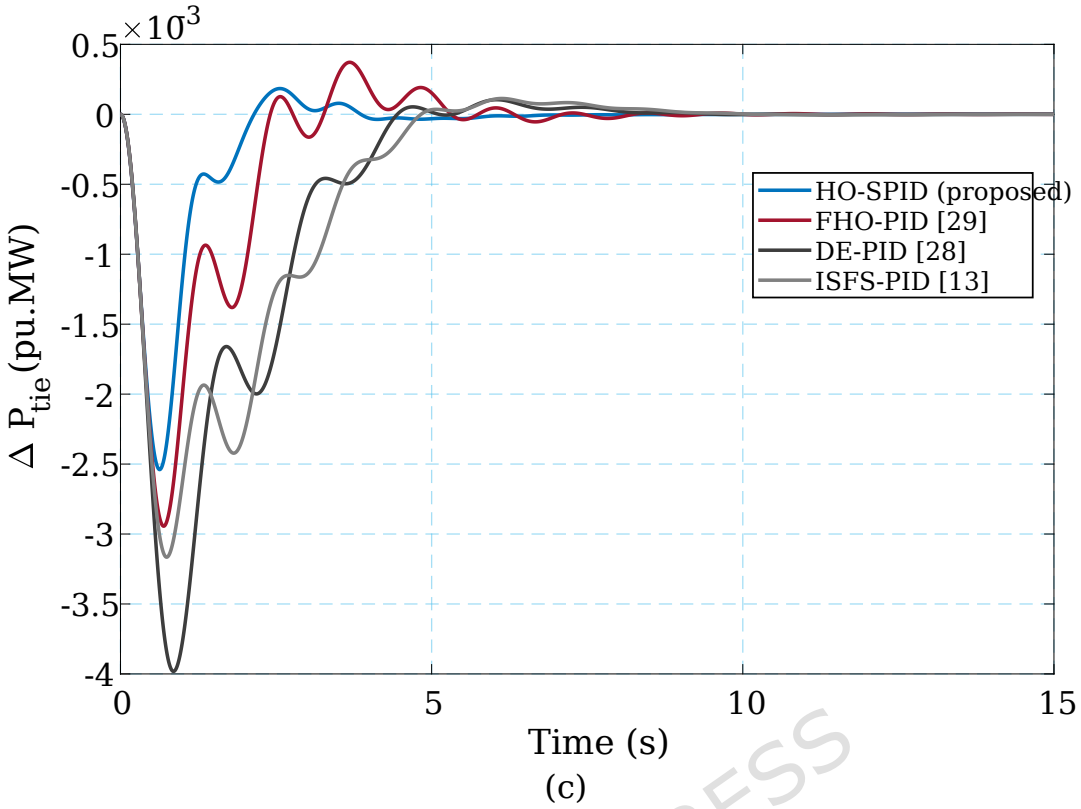

(c)

Figure 7. System responses for Scenario II, a) area-1, b) area-2, c) tie-line

Table 7. Comparison of system performance metrics for different controllers under Scenario II (1% pu load change with GDB effect).

Controller	t_s (s)			MU × 10^{-3} (Hz)		MU (pu.MW)	ITAE
	Δf_1	Δf_2	ΔP_{tie}	Δf_1	Δf_2	ΔP_{tie}	
HO-SPID (proposed)	4.088	3.921	1.943	16.0	9.2	2.5	0.0215
FHO-PID [32]	7.142	7.649	3.980	17.0	11.0	2.94	0.0541
DE-PID [31]	6.666	5.257	4.160	19.3	14.3	4.0	0.0727
ISFS-PID [16]	6.250	6.480	4.400	16.8	11.0	3.1	0.0760

5.4. Scenario III: RES Change

This subsection investigates the impact of RES variations on the baseline system response. To this end, the following conditions are simulated at t = 15 s, and the corresponding system responses are illustrated in Figure 8.

- Area-1: 0.1 pu load increase and 0.2 pu PV power generation.

ARTICLE IN PRESS

- Area-2: 0.1 pu wind power generation.

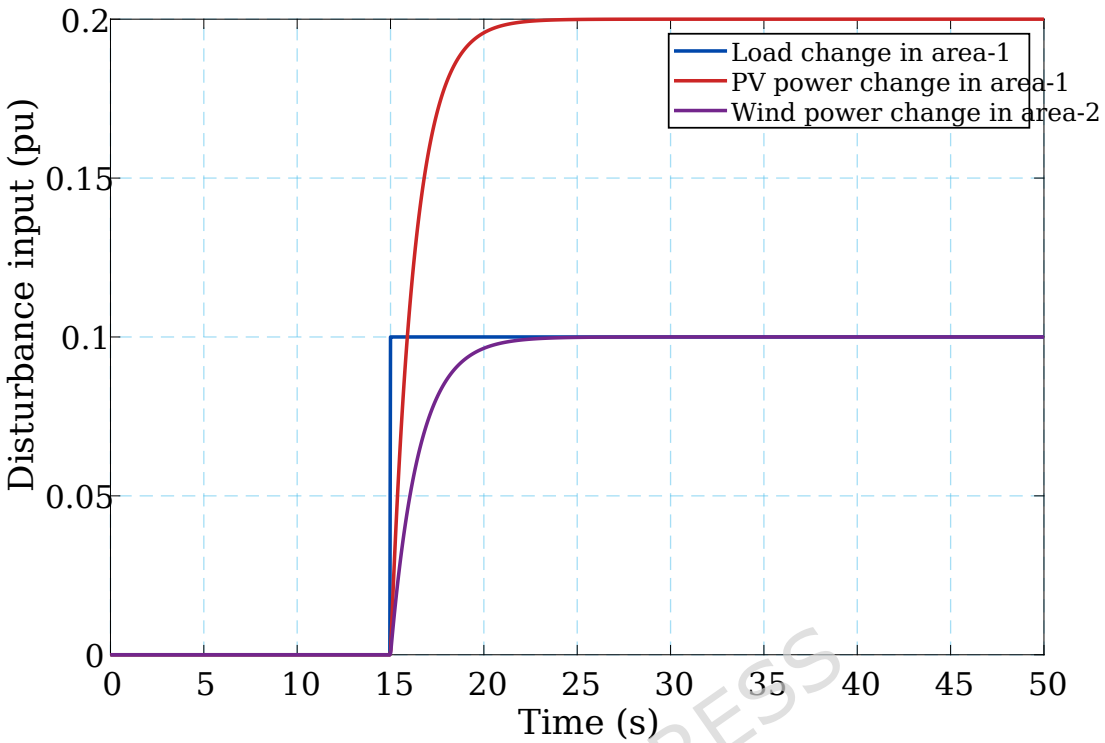

Figure 8. Applied disturbance and RES input profiles for the time-domain simulations

The system responses are illustrated in Figure 9, and the corresponding performance metrics are provided in Table 8. The proposed HO-SPID controller demonstrates consistent superior performance even in the presence of RES fluctuations. As with previous cases, it exhibits better results in terms of settling time, achieving the shortest values for Δf_1, Δf_2, and ΔP_{tie} compared to alternative techniques. In addition, it yields the lowest MU values for all variables and the minimum ITAE index, indicating reduced frequency deviations, smaller tie-line power deviations, and well-damped dynamic responses. Consequently, the HO-SPID controller consistently outperforms alternative techniques across settling time, MU, and ITAE metrics, underscoring its robustness in handling disturbances introduced by RES.

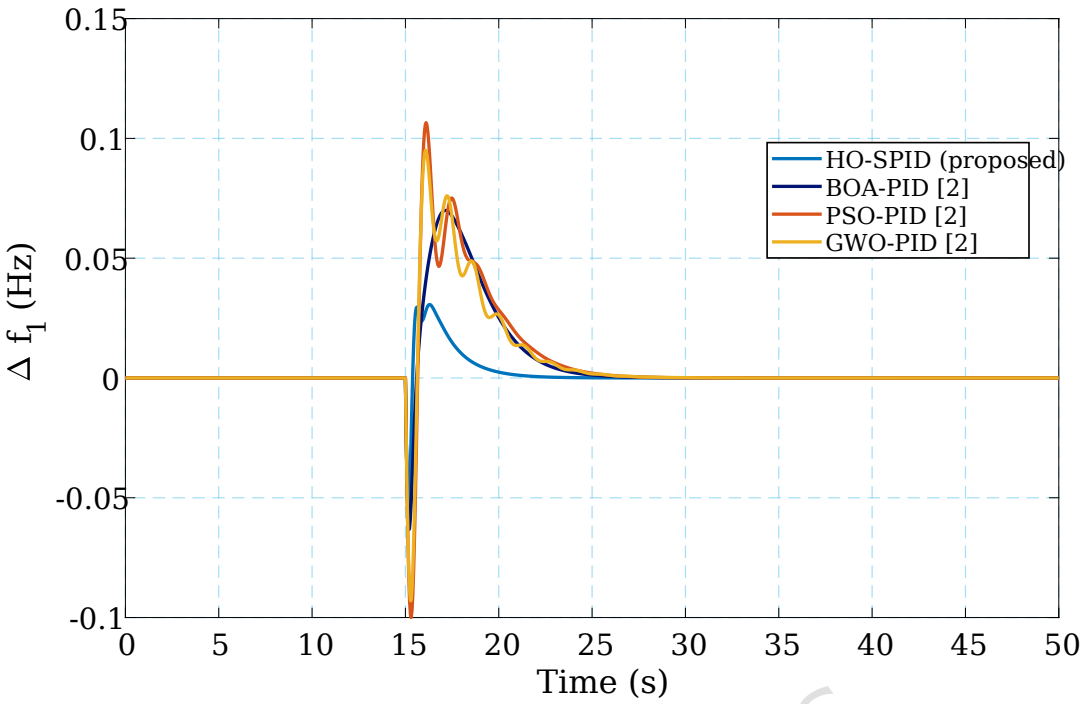

(a)

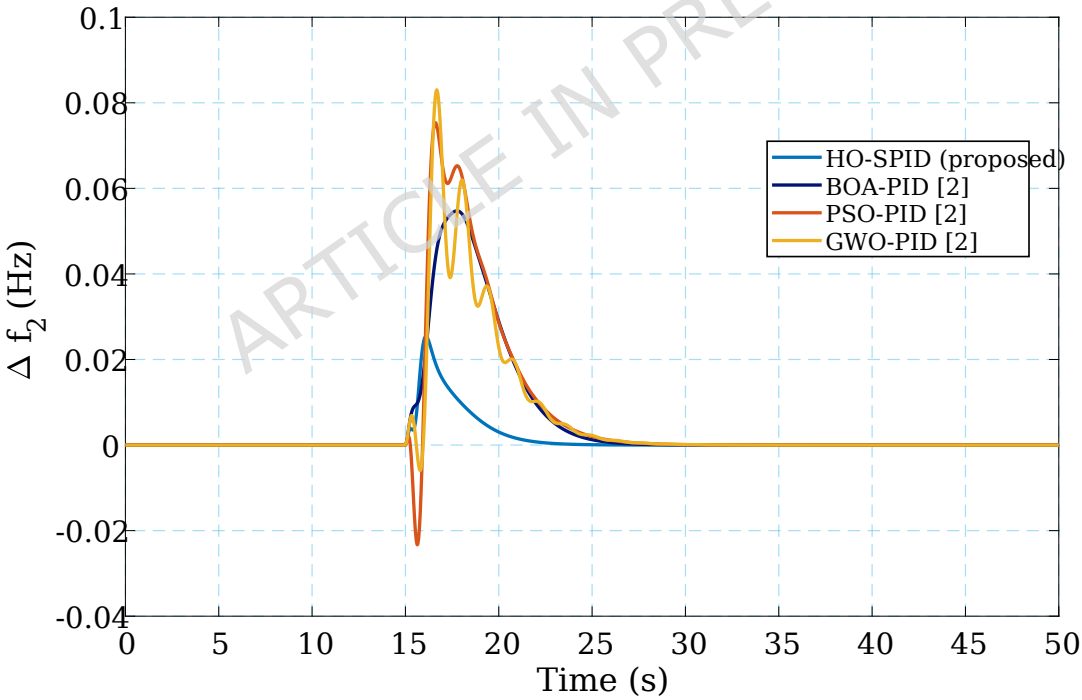

(b)

ARTICLE IN PRESS

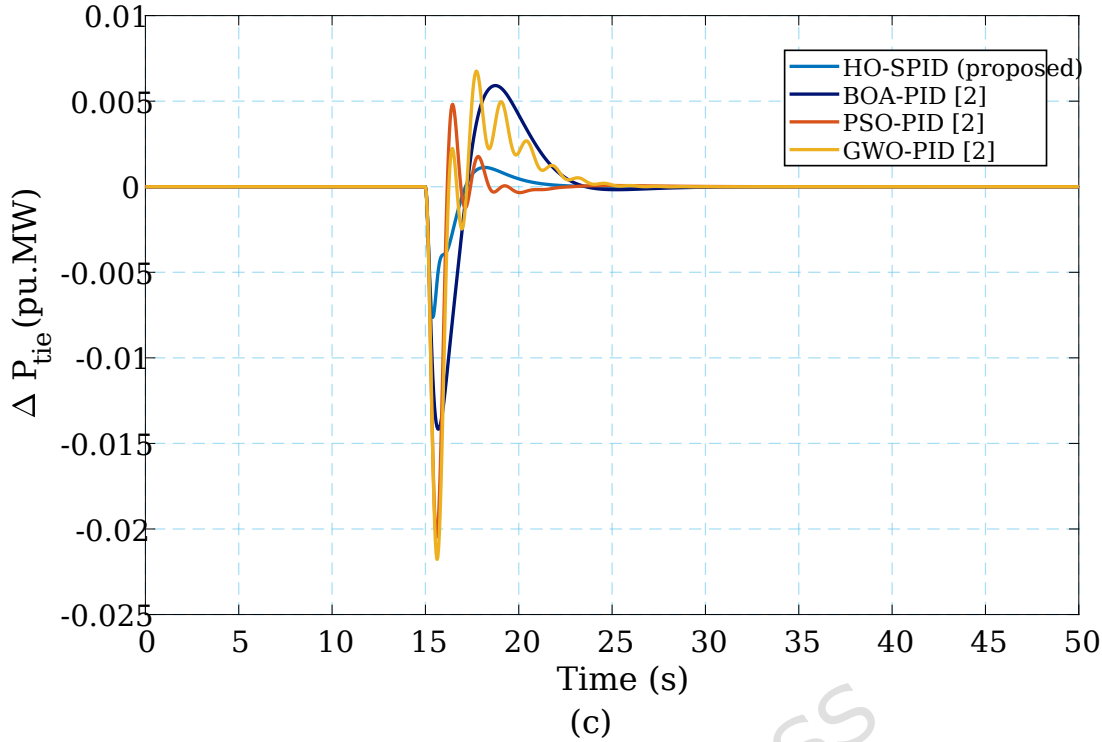

(c)

Figure 9. System responses for Scenario III, a) area-1, b) area-2, c) tie-line

Table 8. Comparison of system performance metrics for different controllers under Scenario III.

Controller	t_s (s)			MU × 10^{-2} (Hz)		MU (pu.MW)	ITAE
	Δf_1	Δf_2	ΔP_{tie}	Δf_1	Δf_2	ΔP_{tie}	
HO-SPID (proposed)	20.276	20.612	16.599	5.45	0	0.76	2.5984
BOA-PID [2]	24.184	24.343	21.183	6.32	0	1.42	10.1293
PSO-PID [2]	25.002	25.002	16.743	9.99	2.33	2.05	11.6412
GWO-PID [2]	24.745	25.186	20.756	9.30	0.60	2.18	10.6230

While the analysis presented above accounts for step changes in WT and PV systems, it is imperative to assess the effectiveness of the controller under more realistic conditions. These conditions reflect the inherent variability of RES owing to changing weather patterns. Consequently, the system undergoes a more comprehensive testing procedure, encompassing concurrent random fluctuations in PV output, wind power generation, and demand variations over a 100-second interval, as depicted

ARTICLE IN PRESS

in Figure 10. Figure 11 illustrates the dynamic responsiveness of the proposed HO-SPID controller under these actual operating conditions. The results demonstrate the efficacy of the controller in preserving system stability, as evidenced by minimal frequency variations and rapid damping of oscillations, even in the presence of continuous fluctuations in generation and demand.

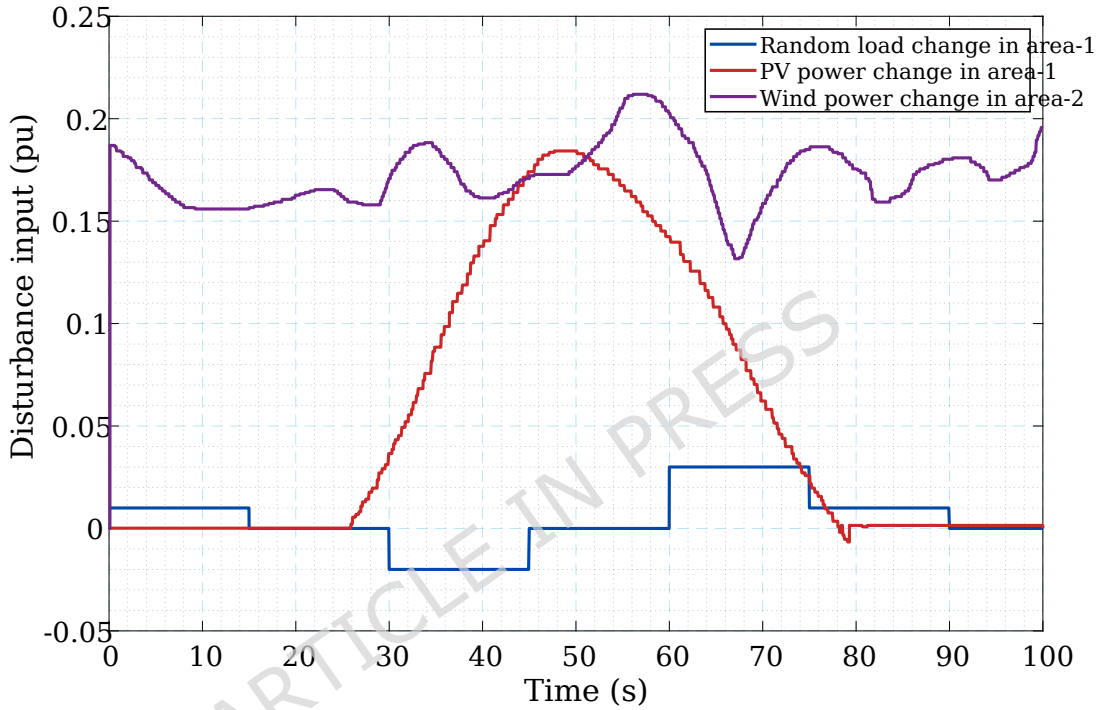

Figure 10. Realistic random disturbance profiles for PV power, wind power, and load change

ARTICLE IN PRESS

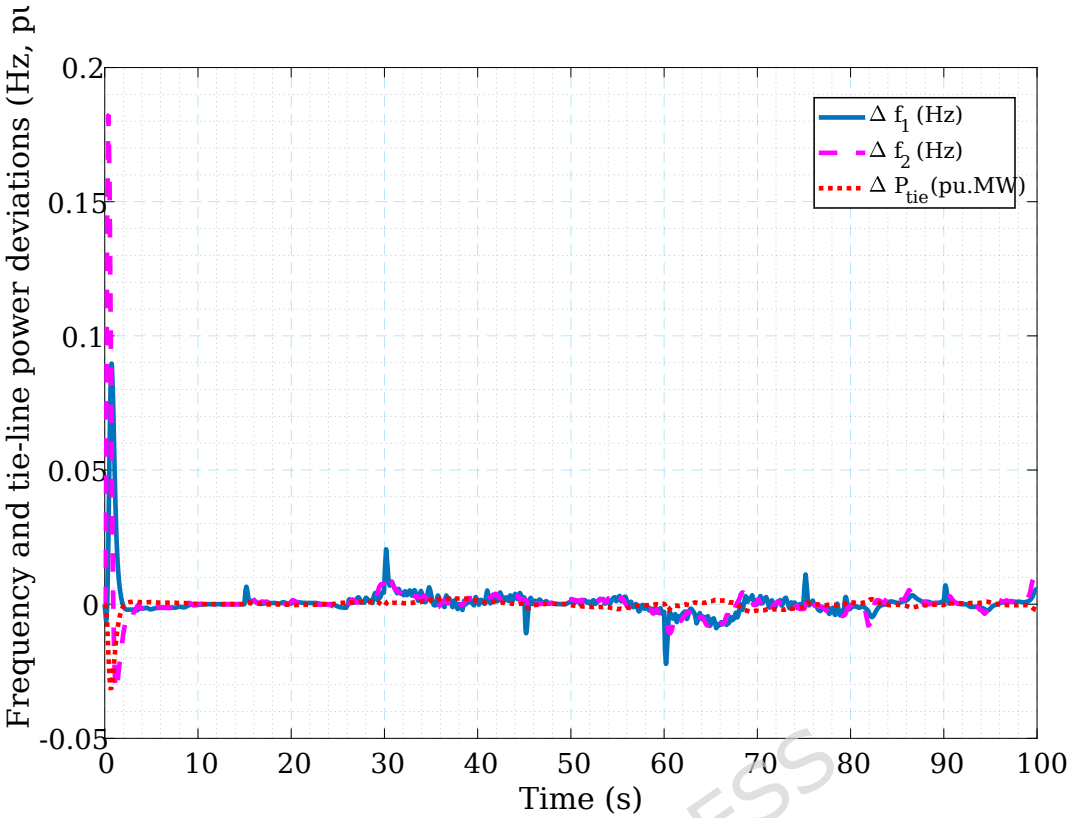

Figure 11. System responses for Scenario III, a) area-1, b) area-2, c) tie-line

ARTICLE IN PRESS

5.5. Scenario IV: Robustness Analysis

Internal or external factors can induce parameter fluctuations, potentially preventing power systems from operating within nominal conditions. Therefore, a robustness test is essential to assess the resilience of the system to such parameter variations. In this context, the system behavior is investigated by simultaneously varying the time constants of system components, along with the governor droop characteristic, frequency bias factor, power system gains, and tie-line synchronization coefficient, by ±25% and ±50%. The corresponding system responses under these combined parameter variation scenarios are illustrated in Figure 12. The results demonstrate that all considered parameter variations yield consistent settling times for the system frequency and tie-line power deviations. This stability indicates that the simultaneous variations in time

ARTICLE IN PRESS

constants and other key system parameters do not adversely affect the settling time, thereby confirming the robustness of the proposed controller. Nevertheless, a discernible correlation exists between the magnitude of the applied parameter variations and the resulting overshoot and undershoot levels in the frequency and tie-line power responses. Specifically, the +25% and +50% variation cases tend to be associated with larger transient deviations, whereas the -25% and -50% cases lead to reduced overshoot and undershoot magnitudes. This behavior is consistent with expected control system dynamics and provides valuable insight into controller performance under parametric uncertainty. Notably, in all tested scenarios, the system responses remain within acceptable operational limits despite these combined parameter variations. This finding is particularly significant as it demonstrates the resilience of the system to parameter uncertainty, which is a crucial attribute for real-world power system applications subject to fluctuating operating conditions.

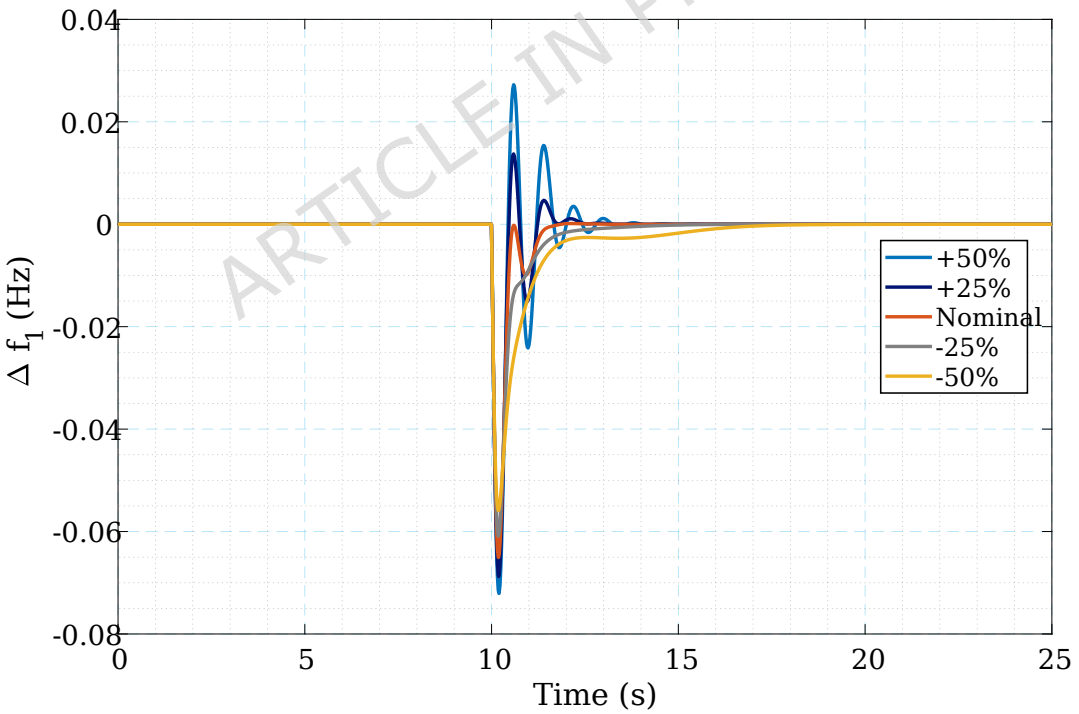

(a)

ARTICLE IN PRESS

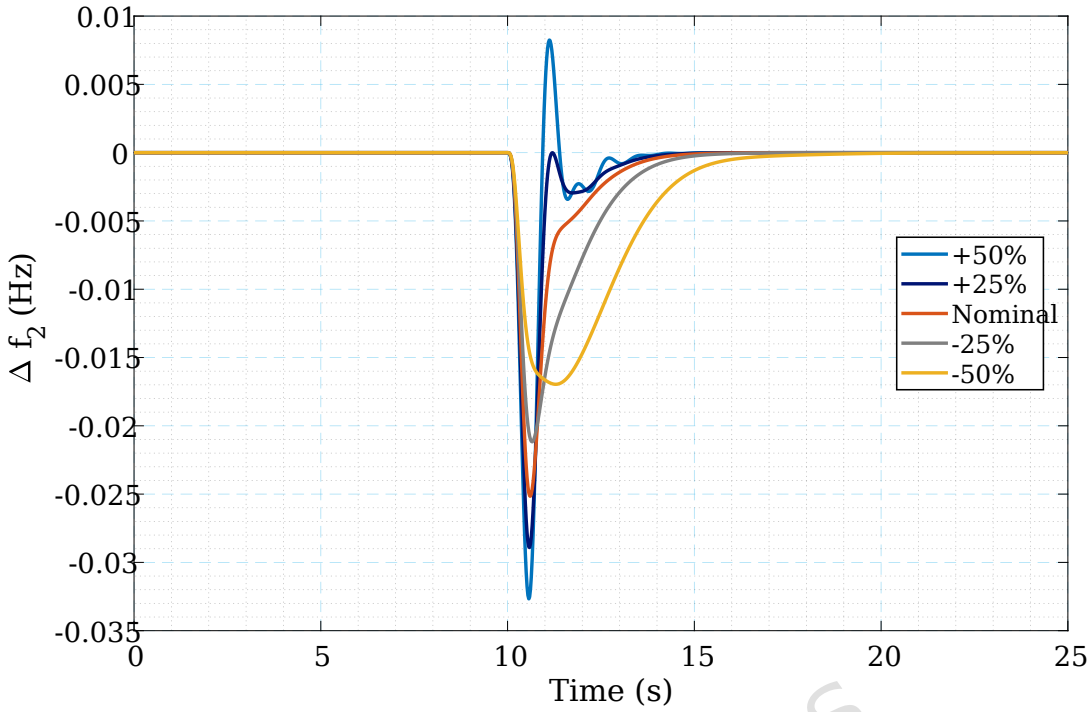

(b)

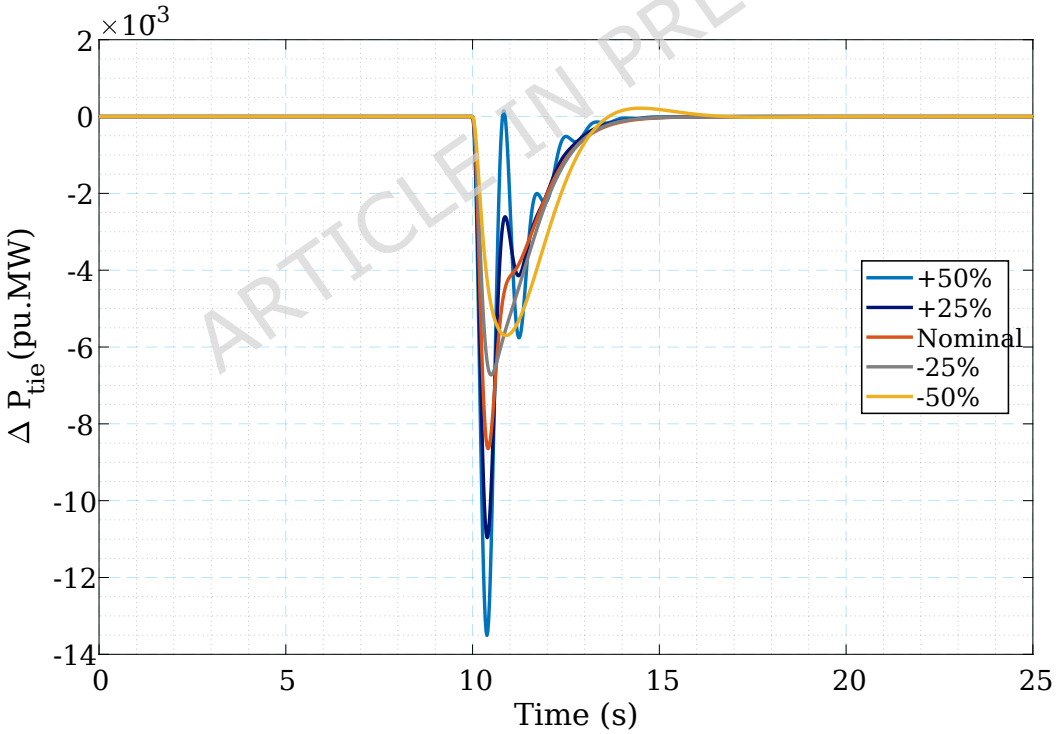

(c)

Figure 12. System responses for Scenario IV, a) area-1, b) area-2, c) tie-line

5.6. Bode Analysis

This subsection presents a detailed analysis of the Bode response of the HO-SPID controller applied to the baseline system, with emphasis on stability characteristics in the frequency domain. Bode analysis provides insight into controller behavior through indicators such as gain margin, phase margin, and bandwidth, which are widely used to assess robustness under different operating conditions and to evaluate disturbance attenuation over a wide frequency range. Classical Bode analysis assumes fixed controller gains; however, the HO-SPID controller employs adaptive gain terms $K_{pv_l}(t)$, $K_{iv_l}(t)$, and $K_{dv_l}(t)$ with $l = 1, 2$ that vary over time. These parameters, defined in Eqs. (11)-(13), adapt in response to system errors and operating condition changes, and their time-varying profiles are shown in Figures 13 and 14. To address this time-varying nature, a frozen-time approach is adopted in which the adaptive gains are fixed at their instantaneous values at selected time instants, allowing the frequency response to be evaluated and classical Bode metrics to be computed as commonly adopted in the literature [39, 40]. Based on this approach, the instantaneous stability properties of the system are assessed at selected time instants, and Bode plots are generated at $t = 10.2$ s and $t = 15$ s, as shown in Figures 15-18.

ARTICLE IN PRESS

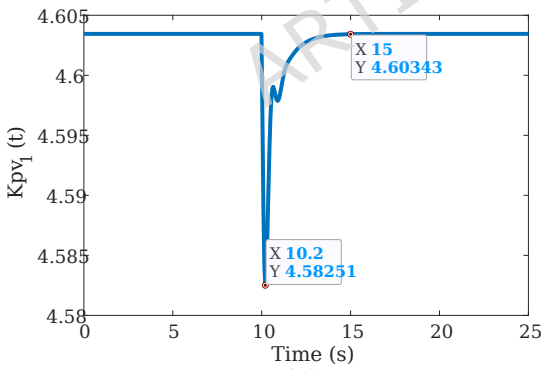

(a)

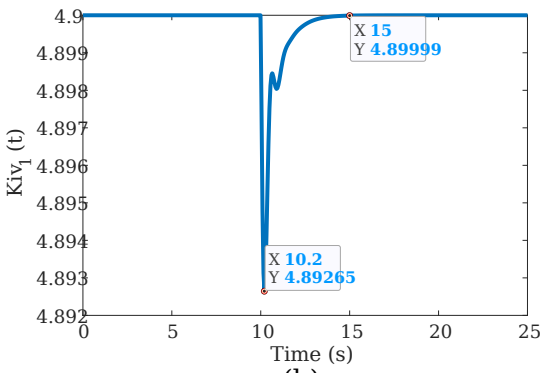

(b)

ARTICLE IN PRESS

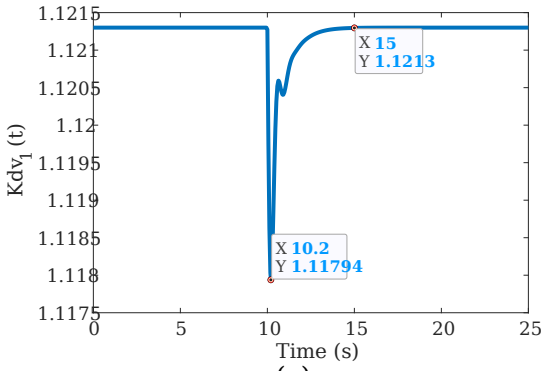

(c)

Figure 13. Time-dependent variation of (a) $K_{pv_1}(t)$, $K_{iv_1}(t)$ and $K_{dv_1}(t)$

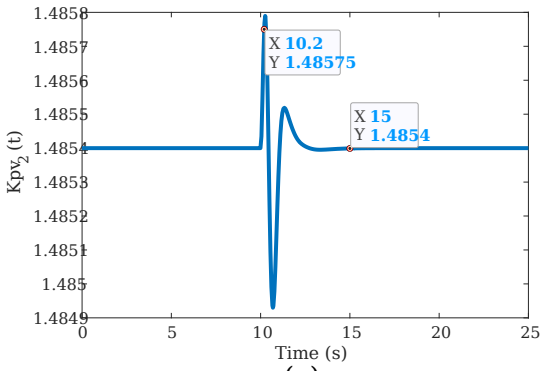

(a)

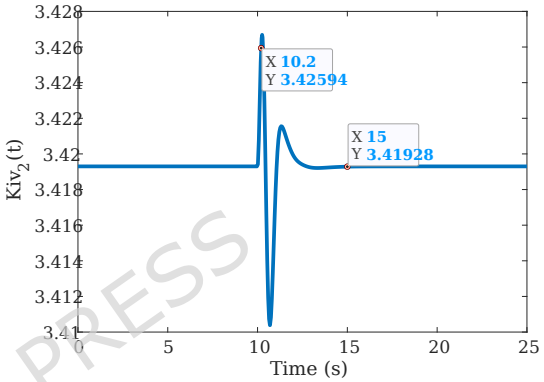

(b)

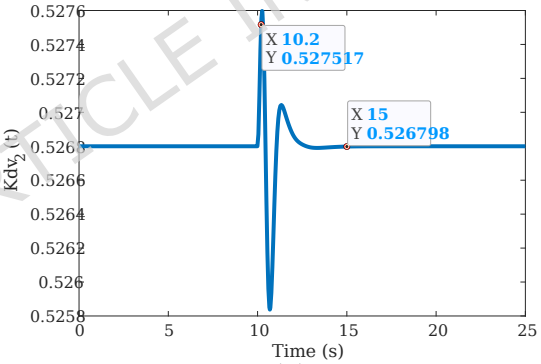

(c)

Figure 14. Time-dependent variation of (a) $K_{pv_2}(t)$, $K_{iv_2}(t)$ and $K_{dv_2}(t)$

ARTICLE IN PRESS

ARTICLE IN PRESS

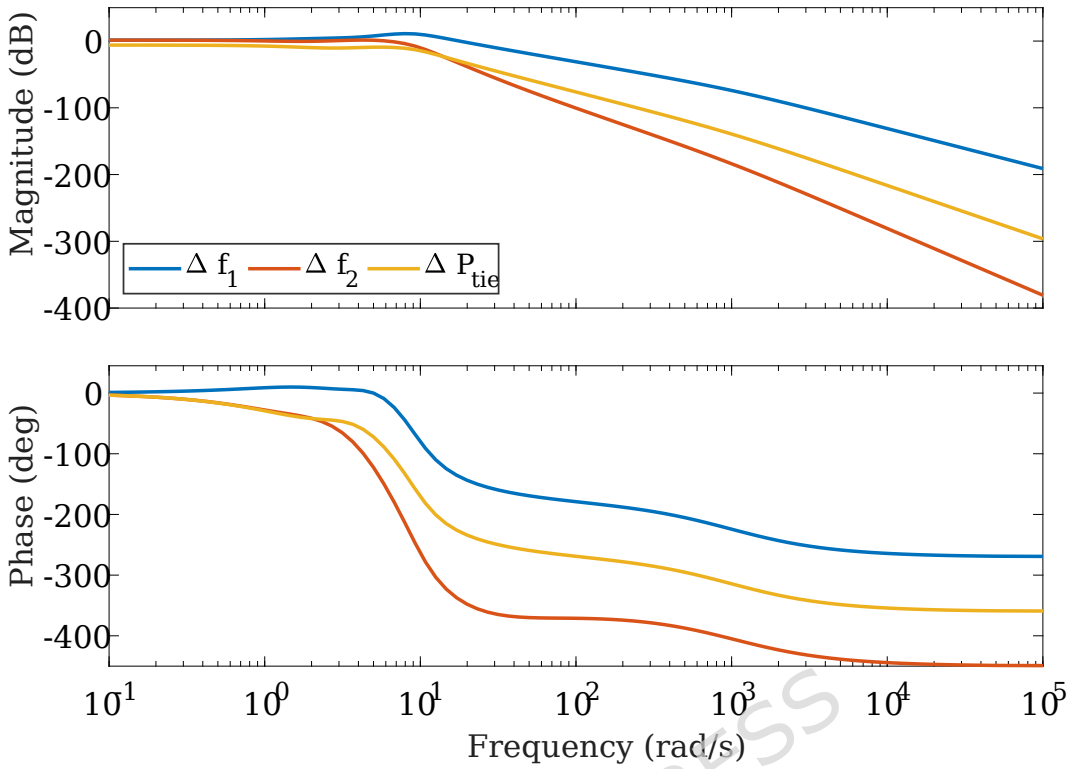

Figure 15. Bode plots of the Scenario 1with HO-SPID$_1$ controller for 10.2 s

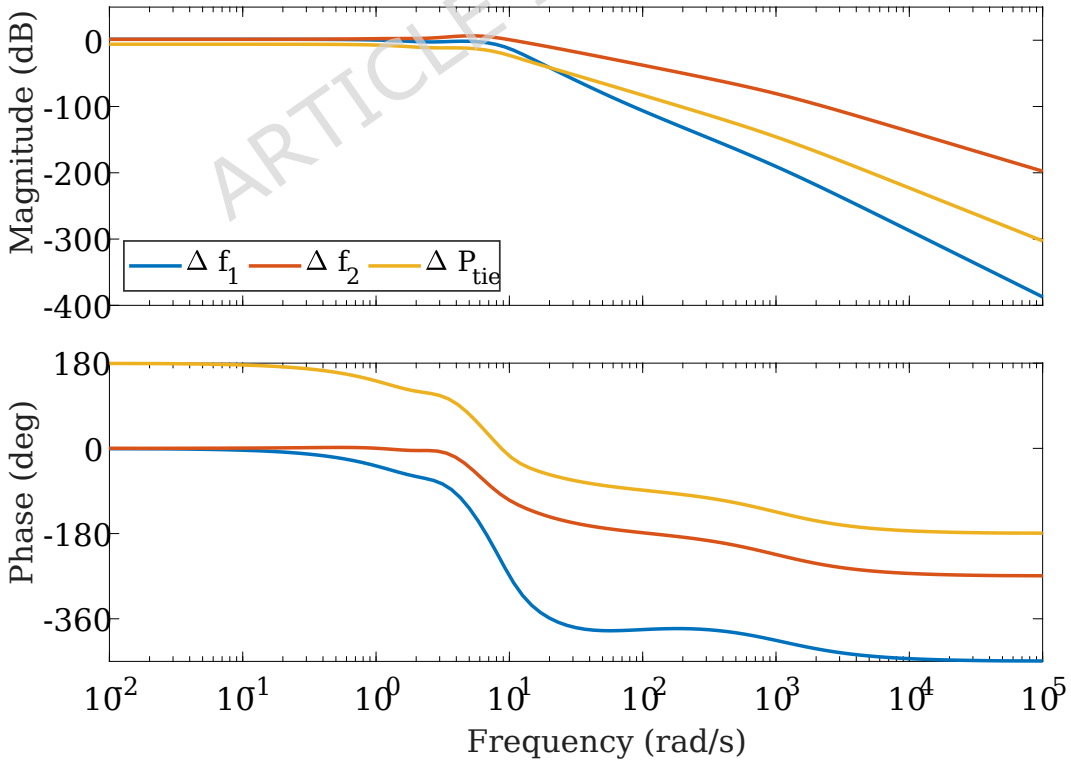

Figure 16. Bode plots of the Scenario 1 with HO-SPID$_2$ controller for 10.2 s

ARTICLE IN PRESS

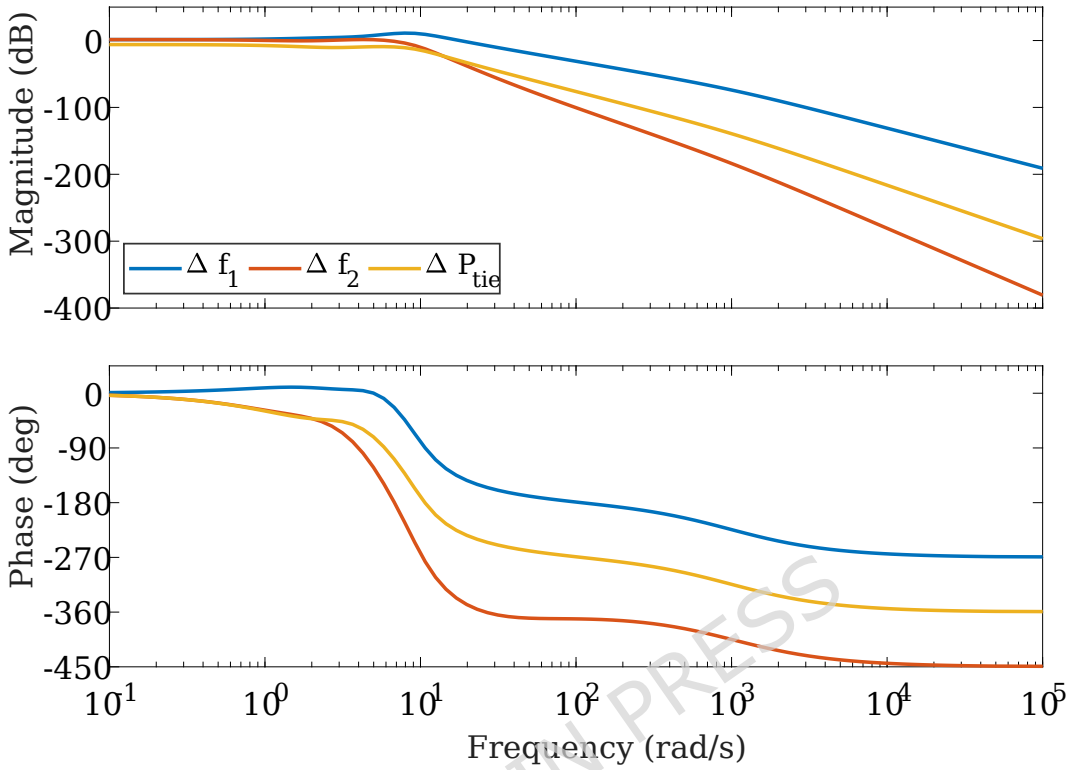

Figure 17. Bode plots of the Scenario 1 with HO: $SPID_1$ controller for 15 s

ARTICLE IN PRESS

ARTICLE IN PRESS

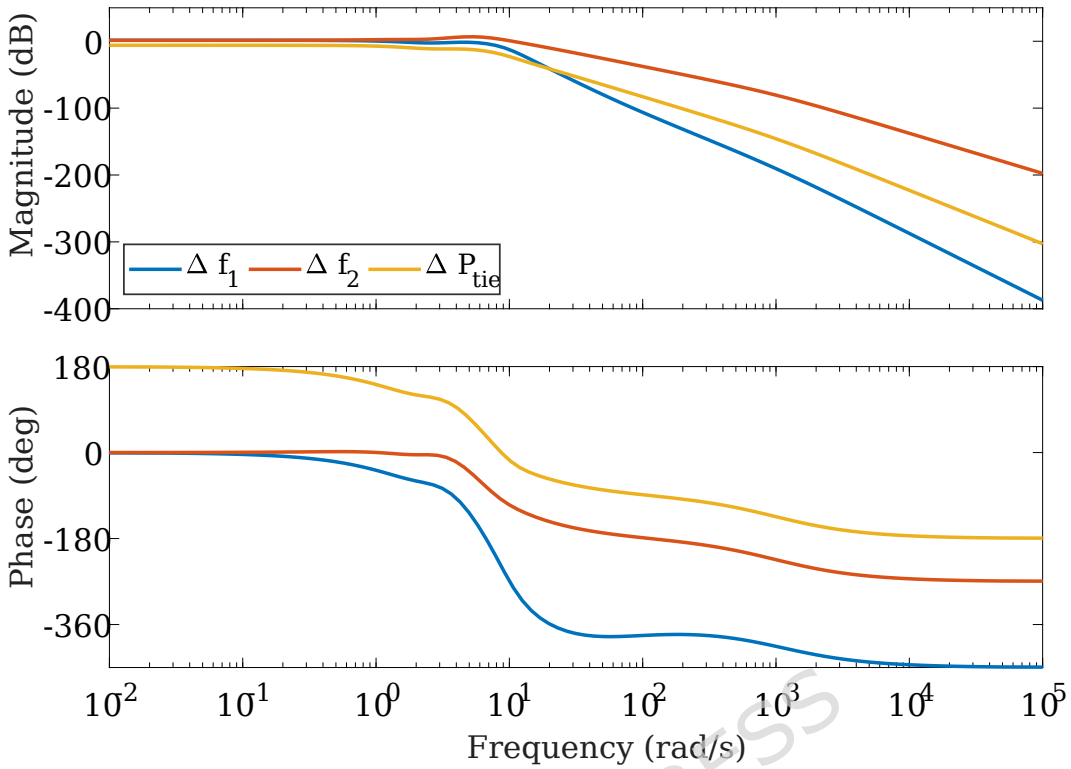

Figure 18. Bode plots of the Scenario 1 with HO: $SPID_2$ controller for 15 s

To quantify the stability characteristics observed in the Bode plots, the numerical values of gain margin, phase margin, and bandwidth are reported in Tables 9 and 10 at two representative time instants, $t = 10.2$ s and $t = 15$ s. For the SPID1 controller, the Δf_1 response exhibits high gain margins (32.5/32.4) and phase margins (42.2/42.1) with wide bandwidths (19.3779/19.4139), indicating fast and well-damped dynamics with strong robustness against phase uncertainties. For the Δf_2 response, the gain margins (1.2/1.21) are moderate and the phase margins (21.2/21.4) remain adequate for phase-delay tolerance; however, the narrower bandwidths (6.9878/6.9867) imply slower dynamics compared to Δf_1. For the ΔP_{tie} response, the gain margins (15.9/15.9) and bandwidths (1.6097/1.6109) indicate stable behavior with limited dynamic speed, while the infinite phase margins reflect excellent phase stability.

For the SPID2 controller, the Δf_1 response shows comparatively lower gain margins (3.55/3.57) but very high phase margins (139/139), suggesting

ARTICLE IN PRESS

strong phase robustness despite the relatively limited gain margin; the narrow bandwidths (1.7511/1.7483) further indicate comparatively slower dynamics in this loop. In contrast, the Δf_2 response achieves high gain margins (40/40) together with phase margins (66.7/66.8) and bandwidths (11.6964/11.6871), reflecting robust stability margins and a faster frequency-domain response than the Δf_1 case. For the ΔP_{tie} response, the gain margins (6.02/6.02) and bandwidths (1.5578/1.5565) indicate stable behavior with limited dynamic speed, while the infinite phase margins again confirm excellent phase stability. Overall, the margins and bandwidth values for both controllers exhibit close agreement between the selected time instants, indicating that the adaptive gain variation does not degrade frequency-domain robustness under the frozen-time evaluation. This observation supports the time-domain results by showing that improved transient performance is achieved without sacrificing classical stability margins.

Table 9. Bode performance indicators of the Scenario 1 with HO-SPID controller for 10.2s

Controller	Gain Margin (dB)	Phase Margin (deg)	Bandwidth
$SPID_1$ controller response to Δf_1	32.5	42.2	19.3779
$SPID_1$ controller response to Δf_2	1.2	21.2	6.9878
$SPID_1$ controller response to ΔP_{tie}	15.9	Inf	1.6097
$SPID_2$ controller to response to Δf_1	3.55	139	1.7511
$SPID_2$ controller to response to Δf_2	40	66.7	11.6964
$SPID_2$ controller to response to ΔP_{tie}	6.02	Inf	1.5578

Table 10. Bode performance indicators of the Scenario 1 with HO: SPID controller for 15s

ARTICLE IN PRESS

Controller	Gain Margin (dB)	Phase Margin (deg)	Bandwidth
$SPID_1$ controller response to Δf_1	32.4	42.1	19.4139
$SPID_1$ controller response to Δf_2	1.21	21.4	6.9867
$SPID_1$ controller response to ΔP_{tie}	15.9	Inf	1.6109
$SPID_2$ controller to response to Δf_1	3.57	139	1.7483
$SPID_2$ controller to response to Δf_2	40	66.8	11.6871
$SPID_2$ controller to response to ΔP_{tie}	6.02	Inf	1.5565

6. Conclusion

In this study, the LFC problem in modern power systems is addressed using an SPID controller whose parameters are optimally tuned via the HO algorithm. As a preliminary step, the optimization capability of the HO algorithm is systematically evaluated using nine benchmark functions and comparatively assessed against several state-of-the-art metaheuristic algorithms. This assessment confirms that HO exhibits strong convergence characteristics and provides an effective and reliable framework for controller parameter optimization. Building on this algorithmic validation, the HO-tuned SPID controller is applied to the LFC problem and its dynamic performance is thoroughly investigated in the time domain. The simulation results demonstrate that the proposed HO-SPID controller significantly reduces the settling time, effectively suppresses undershoot, and consistently achieves improved ITAE performance. Furthermore, the controller efficiently damps frequency and tie-line power oscillations under different disturbance profiles, adapts well to the intermittent and stochastic nature of renewable energy sources, and maintains robust operation even in the presence of considerable parameter uncertainties. To further substantiate the observed time-domain performance, comprehensive Bode analyses are conducted to evaluate the closed-loop stability characteristics in the frequency domain. The resulting gain

ARTICLE IN PRESS

margin, phase margin, and bandwidth values confirm that the proposed controller preserves satisfactory stability margins and robustness over a wide operating range, thereby supporting the effectiveness of the HO-SPID structure from a frequency-domain perspective.

Overall, the results indicate that the HO-SPID controller provides a reliable, stable, and computationally efficient solution for LFC in modern power systems with high renewable energy penetration, thereby enhancing the practical applicability of LFC strategies in renewable-dominated power systems. In future work, real-time hardware implementation and experimental validation of the proposed controller using the OPAL-RT platform will be considered.

Declarations

Acknowledgements: This research was financially supported by the Recep Tayyip Erdoğan University Development Foundation (Grant number: 02025005012474). We sincerely appreciate their support, which contributed significantly to the completion of this study.

Funding: This study has been supported by the Recep Tayyip Erdoğan University Development Foundation (Grant Number: 02025005012474).

Competing interests: The authors have no relevant financial or non-financial interests to disclose.

Author contributions: All authors have contributed equally to this work.

Conflict of Interest: The authors declare that they have no known competing financial interests or personal relationships that could have appeared to influence the work reported in this paper.

Data Availability Statements: The datasets used and/or analysed during the current study available from the corresponding author on reasonable request.

ARTICLE IN PRESS

References

[1] A. Tabak and S. Duman, “Maiden application of TIDμ1NDμ2 controller for effective load frequency control of non-linear two-area power system,” *IET Renewable Power Generation*, vol. 18, no. 7, pp. 1269–1291, May 2024, doi: 10.1049/rpg2.12817.

[2] S. K. Ojha and C. O. Maddela, “Load frequency control of a two-area power system with renewable energy sources using brown bear optimization technique,” *Electrical Engineering*, vol. 106, no. 3, pp. 3589–3613, Jun. 2024, doi: 10.1007/s00202-023-02143-4.

ARTICLE IN PRESS

[3] N. Paliwal, L. Srivastava, and M. Pandit, “Application of grey wolf optimization algorithm for load frequency control in multi-source single area power system,” *Evol Intell*, vol. 15, no. 1, pp. 563–584, Mar. 2022, doi: 10.1007/s12065-020-00530-5.

[4] P. J. Krishna, V. P. Meena, N. Patnana, A. Mathur, and V. P. Singh, “Grey wolf optimizer-assisted R-method-based weighted minimization for automatic generation control in two-area interconnected power system,” *Int J Dyn Control*, vol. 11, no. 4, pp. 1779–1796, Aug. 2023, doi: 10.1007/s40435-022-01070-9.

[5] M. Barakat, A. M. Mabrouk, and A. Donkol, “Optimal design of a cascade controller for frequency stability of photovoltaic–reheat thermal power systems considering nonlinearities,” *Opt Quantum Electron*, vol. 55, no. 4, Apr. 2023, doi: 10.1007/s11082-023-04583-5.

[6] A. K. Mahapatra, P. Samal, S. Mohapatra, P. C. Sahu, and S. Panda, “Analysis of Gaussian fuzzy logic-sliding model control and flexible AC transmission systems controllers for automatic generation control of hybrid power system under chaotic-water cycle algorithm approach,” *International Transactions on Electrical Energy Systems*, vol. 31, no. 12, Dec. 2021, doi: 10.1002/2050-7038.13163.

[7] E. Çelik, N. Öztürk, and E. H. Houssein, “Influence of energy storage device on load frequency control of an interconnected dual-area thermal and solar photovoltaic power system,” *Neural Comput Appl*, vol. 34, no. 22, pp. 20083–20099, Nov. 2022, doi: 10.1007/s00521-022-07558-x.

[8] P. Dahiya and A. K. Saha, “Frequency Regulation of Interconnected Power System Using Black Widow Optimization,” *IEEE Access*, vol. 10, pp. 25219–25236, 2022, doi: 10.1109/ACCESS.2022.3155201.

[9] S. Dewangan, T. Prakash, and V. Pratap Singh, “Design and performance analysis of elephant herding optimization based controller for load frequency control in thermal interconnected power system,” *Optim Control Appl Methods*, vol. 42, no. 1, pp. 144–159, Jan. 2021, doi: 10.1002/oca.2666.

[10] E. Çelik, “Design of new fractional order PI–fractional order PD cascade controller through dragonfly search algorithm for advanced load frequency control of power systems,” *Soft comput*, vol. 25, no. 2, pp. 1193–1217, Jan. 2021, doi: 10.1007/s00500-020-05215-w.

[11] Limon, M. F. A., Upoma, R. S., Sinha, N., Swarna, S. R., Nath, B. K., Khanum, K., ... & Iqbal, M. S. (2025). Grey wolf optimization-based fuzzy-PID controller for load frequency control in multi-area power systems. *Journal of Automation and Intelligence*

[12] G. Sahoo, R. K. Sahu, S. Panda, N. R. Samal, and Y. Arya, “Modified Harris Hawks Optimization-Based Fractional-Order Fuzzy PID Controller for Frequency Regulation of Multi-Micro-Grid,” *Arab J Sci*

ARTICLE IN PRESS

Eng, vol. 48, no. 11, pp. 14381–14405, Nov. 2023, doi: 10.1007/s13369-023-07613-2.

[13] Jalilian, M., Rastgou, A., Kharrati, S., & Hosseini-Hemati, S. (2025). Load Frequency Control Resilience of Hybrid Power System with Renewable Energy Sources and Superconducting Magnetic Energy Storage Using FO-Fuzzy-PID Controller. *Results in Engineering*, 105961.

[14] Nayak, P. C., Prusty, R. C., & Panda, S. (2024). Adaptive fuzzy approach for load frequency control using hybrid moth flame pattern search optimization with real time validation. *Evolutionary Intelligence*, *17*(2), 1111-1126.

[15] A. Deepa *et al.*, "An optimized frequency control of green energy integrated microgrid power system using modified SSO Algorithm," *Soft comput*, vol. 28, no. 9–10, pp. 6423–6446, May 2024, doi: 10.1007/s00500-023-09504-y.

[16] E. Çelik, "Improved stochastic fractal search algorithm and modified cost function for automatic generation control of interconnected electric power systems," *Eng Appl Artif Intell*, vol. 88, Feb. 2020, doi: 10.1016/j.engappai.2019.103407.

[17] D. Sibtain, T. Rafiq, M. H. Bhatti, S. Shahzad, and H. Kilic, "Frequency stabilization for interconnected renewable based power system using cascaded model predictive controller with fractional order PID controller," *IET Renewable Power Generation*, vol. 17, no. 16, pp. 3836–3855, Dec. 2023, doi: 10.1049/rpg2.12885.

[18] A. E. Khalil, T. A. Boghdady, M. H. Alham, and D. K. Ibrahim, "Enhancing the Conventional Controllers for Load Frequency Control of Isolated Microgrids Using Proposed Multi-Objective Formulation via Artificial Rabbits Optimization Algorithm," *IEEE Access*, vol. 11, pp. 3472–3493, 2023, doi: 10.1109/ACCESS.2023.3234043.

[19] R. El-Sehiemy, A. Shaheen, A. Ginidi, and S. F. Al-Gahtani, "Proportional-Integral-Derivative Controller Based-Artificial Rabbits Algorithm for Load Frequency Control in Multi-Area Power Systems," *Fractal and Fractional*, vol. 7, no. 1, Jan. 2023, doi: 10.3390/fractalfract7010097.

[20] R. K. Khadanga, A. Kumar, and S. Panda, "A novel modified whale optimization algorithm for load frequency controller design of a two-area power system composing of PV grid and thermal generator," *Neural Comput Appl*, vol. 32, no. 12, pp. 8205–8216, Jun. 2020, doi: 10.1007/s00521-019-04321-7.

[21] P. R. Sahu *et al.*, "Effective Load Frequency Control of Power System with Two-Degree Freedom Tilt-Integral-Derivative Based on Whale Optimization Algorithm," *Sustainability (Switzerland)*, vol. 15, no. 2, 2023, doi: 10.3390/su15021515.

ARTICLE IN PRESS

[22] E. Çelik, N. Öztürk, Y. Arya, and C. Ocak, “(1 + PD)-PID cascade controller design for performance betterment of load frequency control in diverse electric power systems,” *Neural Comput Appl*, vol. 33, no. 22, pp. 15433–15456, Nov. 2021, doi: 10.1007/s00521-021-06168-3.

[23] A. A. Abou El-Ela, R. A. El-Sehiemy, A. M. Shaheen, and A. E. G. Diab, “Design of cascaded controller based on coyote optimizer for load frequency control in multi-area power systems with renewable sources,” *Control Eng Pract*, vol. 121, Apr. 2022, doi: 10.1016/j.conengprac.2021.105058.

[24] E. Sahin, “Design of an Optimized Fractional High Order Differential Feedback Controller for Load Frequency Control of a Multi-Area Multi-Source Power System with Nonlinearity,” *IEEE Access*, vol. 8, pp. 12327–12342, 2020, doi: 10.1109/ACCESS.2020.2966261.

[25] M. Khamies, G. Magdy, A. Selim, and S. Kamel, “An improved Rao algorithm for frequency stability enhancement of nonlinear power system interconnected by AC/DC links with high renewables penetration,” *Neural Comput Appl*, vol. 34, no. 4, pp. 2883–2911, Feb. 2022, doi: 10.1007/s00521-021-06545-y.

[26] A. Daraz, S. A. Malik, A. Basit, S. Aslam, and G. Zhang, “Modified FOPID Controller for Frequency Regulation of a Hybrid Interconnected System of Conventional and Renewable Energy Sources”, Fractal Fract. 2023, 7, 89. https://doi.org/10.3390/fractalfract7010089

[27] P. Zhang, A. Daraz, S. A. Malik, C. Sun, A. Basit, and G. Zhang, “Multi-resolution based PID controller for frequency regulation of a hybrid power system with multiple interconnected systems”, Front. Energy Res, Volume 10 - 2022 | https://doi.org/10.3389/fenrg.2022.1109063

[28] P. K. Vidyarthi, A. Kumar, and S. Raj, “Chaos quasi-opposition sea-horse based modified new tilt controller designed for multi-area deregulated AGC using deep learning against cyber-attacks”, Chaos Solitons Fractals, vol. 188, Nov. 2024, doi: 10.1016/j.chaos.2024.115542

[29] D. H. Wolpert and W. G. Macready, “No Free Lunch Theorems for Optimization,” 1997.

[30] M. H. Amiri, N. Mehrabi Hashjin, M. Montazeri, S. Mirjalili, and N. Khodadadi, “Hippopotamus optimization algorithm: a novel nature-inspired optimization algorithm,” *Sci Rep*, vol. 14, no. 1, Dec. 2024, doi: 10.1038/s41598-024-54910-3.

[31] Mohanty B, Panda S, Hota PK (2014) Differential evolution algorithm based automatic generation control for interconnected power systems with non-linearity. Alex Eng J 53:537–552

ARTICLE IN PRESS

[32] Awal, M., Atim, M. R., Wanzala, J. N., Obungoloch, J., & Barakat, M. (2025). Fire hawk optimizer adjusted PD-PI cascade controller for automatic generation control of IPS. Electrical Engineering, 1-22.

[33] Ates, B. B. Alagoz, C. Yeroglu, and H. Alisoy, “Sigmoid based PID controller implementation for rotor control,” 2015 European Control Conference (ECC), Jul. 2015. doi:10.1109/ecc.2015.7330586

[34] Azizi, M., Talatahari, S., & Gandomi, A. H. (2023). Fire Hawk Optimizer: A novel metaheuristic algorithm. Artificial Intelligence Review, 56(1), 287-363.

[35] Prakash, T., Singh, P. P., Singh, V. P., & Singh, S. N. (2023). A novel brown-bear optimization algorithm for solving economic dispatch problem. In Advanced control & optimization paradigms for energy system operation and management (pp. 137-164). River Publishers.

[36] Mirjalili, S., Mirjalili, S. M., & Lewis, A. (2014). Grey wolf optimizer. Advances in engineering software, 69, 46-61.

[37] Kennedy, J., & Eberhart, R. (1995, November). Particle swarm optimization. In Proceedings of ICNN'95-international conference on neural networks (Vol. 4, pp. 1942-1948). ieee.

[38] Storn, R., & Price, K. (1997). Differential evolution–a simple and efficient heuristic for global optimization over continuous spaces. Journal of global optimization, 11(4), 341-359.

[39] Sahin, A. K., Cavdar, B., & Ayas, M. S. (2024). An adaptive fractional controller design for automatic voltage regulator system: Sigmoid-based fractional-order PID controller. Neural Computing and Applications, 36(23), 14409-14431

[40] Suid, M. H., & Ahmad, M. A. (2022). Optimal tuning of sigmoid PID controller using nonlinear sine cosine algorithm for the automatic voltage regulator system. *ISA transactions*, *128*, 265-286.

ARTICLE IN PRESS